

A meshless generalized finite difference method for solving the Stokes-Darcy coupled problem in static and moving systems

Yanan Xing^a, Haibiao Zheng^{a,*}

^a*School of Mathematical Sciences, Key Laboratory of MEA(Ministry of Education), Shanghai Key Laboratory of PMMP, East China Normal University, shanghai, 200241, China*

ARTICLE INFO

Keywords:

Meshless method
Generalized Finite Difference Method
Stokes-Darcy coupled problem
Static and moving systems
Poisson Pressure Equation
Closed interface shape

ABSTRACT

In this paper, a meshless Generalized Finite Difference Method (GFDM) is proposed to deal with the Stokes-Darcy coupled problem with the Beavers-Joseph-Saffman (BJS) interface conditions. Some high order GFDMs are proposed to show the advantage of the high order GFDM for the Stokes-Darcy coupled problem, which is that the high order method has high order accuracy and the convergence order. Some Stokes-Darcy coupled problems with closed interfaces, which has more complex geometric shape, are given to show the advantage of the GFDM for the complex interface. The interface location has been changed to show the influence of the interface location for the Stokes-Darcy coupled problem. The BJS interface conditions has related to the partial derivatives of unknown variables and the GFDM has advantage in dealing with the interface conditions with the jump of derivatives. Four numerical examples have been provided to verify the existence of the good performance of the GFDM for the Stokes-Darcy coupled problems, including that the simplicity, accuracy, and stability in static and moving systems. Especially, the GFDM has the tolerance of the large jump. The Neumann boundary condition is used in numerical simulations.

1. Introduction

The Stokes-Darcy coupled problem can accurately describe the motion of fluids in open spaces and the seepage process in porous media, and is widely used in the study of groundwater flow in aquifers, oil and gas extraction processes, and so on.

In the past few years, a number of efficient numerical methods have been proposed to solve the Stokes-Darcy coupled problem. For instance, the coupled finite element method[1,2], the stabilized mixed finite element method[3,4], the finite element based double or multiple mesh method[5-8], the Lagrangian multiplier method[9], the partitioned time stepping or operator splitting method[10-13], and the domain decomposition method[14-19]. In particular, Sun et al.[20,21] used the domain decomposition method to solve the fully-mixed Stokes-Darcy coupling problem, and further used the Robin type domain decomposition algorithm based on two-grid techniques to solve the Stokes-Darcy coupled problem. Chen et al.[22] analyzed the Stokes-Darcy coupled problem by using a parallel Robin-Robin type domain decomposition algorithm. Li et al.[23] used a stabilized finite element method based on two local Gauss integrations to solve the coupled Stokes-Darcy problem. Li et al.[24] used an augmented Cartesian grid method to solve Stokes-Darcy fluid-structure interaction problems with closed interfaces. These computational methods based on finite element methods have contributed to the processing of Stokes-Darcy coupled models, but the generation and reconstruction of meshes have significantly increased the computational workload significantly. Therefore, experts are actively exploring meshless methods to solve Stokes-Darcy coupled models and have made some progress.

There are several meshless methods that have been successfully proposed to solve the Stokes-Darcy coupled problem. For instance, Safarpour et al. [25] proposed a coupled method called the Radial Basis Function-Finite Difference(RBF-FD) to solve the Stokes-Darcy equations. Pu et al. [26] proposed a meshless deep learning method based on a physics-informed neural network to solve coupled Stokes-Darcy equations with Beavers-Joseph-Saffman interface conditions. Yue et al. [27] proposed a coupled deep neural networks to solve the time-dependent coupled Stokes-Darcy problems. Although these meshed and meshless methods have been developed for solving the Stokes-Darcy coupled problem, it is still a changing task to accurately, efficiently and stably solve this classical Stokes-Darcy

*Corresponding author

✉ hbzheng@math.ecnu.edu.cn (H. Zheng)
ORCID(s):

coupled problem. In this work, we will consider the Generalized Finite Difference Method (GFDM) for solving the Stokes-Darcy coupled problems.

The GFDM, which is based on Taylor series expansions and weighted moving square (MLS) approximation, is truly free from mesh generation and numerical quadrature. The basic concept of the GFDM was proposed by Orkisz and Lizska [28] in the early eighties. The GFDM was improved and developed by Benito et al. [29,30] and then extended to various mechanical problems [31,32]. Later, the GFDM was developed by Fan et al. [33] and Gu et al. [34] to solve the ill-posed inverse problem. More recently, the GFDM has been applied to the interface problem in static and moving systems [35-38], the elasticity interface problem[39], the biharmonic interface problems[40], the Stokes equations[41] and the Stokes interface problem[42], and so on. For especially, the Stokes equation and the Stokes interface problems used a mixed boundary condition (MBC) to deal with the pressure oscillations in the Stokes equations, and in this paper, we will adopt a pressure Poisson equation to reduce the pressure oscillations and use the GFDM to solve the Stokes-Darcy coupled problem.

The rest of the paper is structured as follows: Section 2 introduces the model of Stokes-Darcy coupled problem. Section 3 presents the procedure of the GFDM, the handling skill for the Stokes-Darcy coupled problem, and the GFDM for the Stokes-Darcy coupled problem. In Section 4, convergence analysis is proposed. In Section 5, four numerical examples are presented to verify the accuracy, high efficiency and stability of the proposed methods. Finally, a conclusion is presented in Section 6.

2. The Stokes-Darcy coupled problem

We consider the Stokes equations governed by the fluid velocity $\mathbf{u}_f(x, y)$ and pressure $p(x, y)$ in Ω_f :

$$-\nabla \cdot T(\mathbf{u}_f, p_f) = \mathbf{f}_f, \quad \text{in } \Omega_f, \quad (1)$$

$$\nabla \cdot \mathbf{u}_f = 0, \quad \text{in } \Omega_f, \quad (2)$$

where $T = -pI + 2vD(\mathbf{u}_f)$ denotes the stress tensor, and $D(\mathbf{u}_f) = \frac{1}{2}(\nabla \mathbf{u}_f + (\nabla \mathbf{u}_f)^T)$ represents the deformation tensor, in which v is the kinematic viscosity of the fluid, \mathbf{f}_f is the external body force.

The Darcy equations governed by the Darcy velocity $\mathbf{u}_p(x, y)$ and the piezometric head $\phi(x, y)$ in Ω_p :

$$\mathbf{u}_p = -K \nabla \phi, \quad \text{in } \Omega_p, \quad (3)$$

$$\nabla \cdot \mathbf{u}_p = \mathbf{f}_p, \quad \text{in } \Omega_p, \quad (4)$$

in which K denotes the hydraulic conductivity tensor, \mathbf{f}_p is the external body force. And the Beavers-Joseph-Saffman(-Jones) coupling conditions on the interface Γ :

$$\mathbf{u}_f \cdot \mathbf{n}_f + \mathbf{u}_p \cdot \mathbf{n}_p = 0, \quad \text{on } \Gamma, \quad (5)$$

$$\mathbf{n}_f \cdot T(\mathbf{u}_f, p_f) \cdot \mathbf{n}_f = g\phi, \quad \text{on } \Gamma, \quad (6)$$

$$\mathbf{n}_f \cdot T(\mathbf{u}_f, p_f) \cdot \boldsymbol{\tau}_i = \frac{v\alpha\sqrt{d}}{\sqrt{\text{trace}(\Pi)}} \mathbf{u}_f \cdot \boldsymbol{\tau}_i, 1 \leq i \leq d-1, \quad \text{on } \Gamma, \quad (7)$$

where \mathbf{n}_f and \mathbf{n}_p denote the unit outer normal to the fluid and the porous media regions at the interface Γ , respectively. $\boldsymbol{\tau}_i (i = 1, 2, \dots, d-1)$ denote mutually orthogonal unit tangential vectors to the interface Γ and the constant parameter α depends on v and K . For simplicity, we assume that the hydraulic head ϕ and the fluid velocity \mathbf{u}_f satisfy a homogeneous Dirichlet condition except on Γ , unless they are stated otherwise:

$$\phi = 0, \quad \text{on } \partial\Omega_p \setminus \Gamma, \quad (8)$$

$$\mathbf{u}_f = 0, \quad \text{on } \partial\Omega_f \setminus \Gamma. \quad (9)$$

We can see that the Eq.(1) can be rewritten as the follows

$$-\nabla \cdot (v(\nabla \mathbf{u}_f + (\nabla \mathbf{u}_f)^T)) + \nabla \cdot p = \mathbf{f}_f, \quad \text{in } \Omega_f. \quad (10)$$

Note that Eq.(2) doesn't have any information about the pressure p . Therefore, we use the classical pressure poisson equation from [43], which finds divergence on both sides of the equal sign for Eq.(10), then

$$-\nabla \cdot (v(\Delta \mathbf{u}_f + (\Delta \mathbf{u}_f)^T)) + \Delta p = \nabla \cdot \mathbf{f}_f, \text{ in } \Omega_f. \quad (11)$$

Due to Eq.(2), the above equation can be simplified as follows

$$\Delta p = \nabla \cdot \mathbf{f}_f, \text{ in } \Omega_f, \quad (12)$$

Therefore, the Eq.(2) can be exchange into the following part

$$\Delta p = \nabla \cdot \mathbf{f}_f, \text{ in } \Omega_f, \quad (13)$$

$$\nabla \cdot \mathbf{u}_f = 0, \text{ on } \partial\Omega_f. \quad (14)$$

In the boundary part of the above equations, we adopt the following scheme

$$\nabla \cdot \mathbf{u}_f + p - p = 0, \text{ on } \partial\Omega_f, \quad (15)$$

then a new boundary condition can be obtained

$$\nabla \cdot \mathbf{u}_f + p = p, \text{ on } \partial\Omega_f. \quad (16)$$

For simplicity, the governing equation and the interface condition can be described by matrix components as follows:

Stokes equation:

$$-2v \frac{\partial^2 u_1(x, y)}{\partial x^2} - v \frac{\partial^2 u_1(x, y)}{\partial y^2} - v \frac{\partial^2 u_2(x, y)}{\partial x \partial y} + \frac{\partial p(x, y)}{\partial x} = f_1(x, y), \text{ in } \Omega_f, \quad (17)$$

$$-v \frac{\partial^2 u_2(x, y)}{\partial x^2} - 2v \frac{\partial^2 u_2(x, y)}{\partial y^2} - v \frac{\partial^2 u_1(x, y)}{\partial x \partial y} + \frac{\partial p(x, y)}{\partial y} = f_2(x, y), \text{ in } \Omega_f, \quad (18)$$

$$\frac{\partial^2 p(x, y)}{\partial x^2} + \frac{\partial^2 p(x, y)}{\partial y^2} = 0, \text{ in } \Omega_f, \quad (19)$$

Darcy equation:

$$-K \frac{\partial^2 \phi(x, y)}{\partial x^2} - K \frac{\partial^2 \phi(x, y)}{\partial y^2} = f_p(x, y), \text{ in } \Omega_p, \quad (20)$$

with interface condition:

$$u_1(x, y)n_{f_1} + u_2(x, y)n_{f_2} - K \frac{\partial \phi(x, y)}{\partial x} n_{p_1} - K \frac{\partial \phi(x, y)}{\partial y} n_{p_2} = 0, \text{ on } \Gamma, \quad (21)$$

$$p(x, y) - 2v \frac{\partial u_1(x, y)}{\partial x} (n_{f_1})^2 - 2v \frac{\partial u_1(x, y)}{\partial y} n_{f_2} n_{f_1} - 2v \frac{\partial u_2(x, y)}{\partial x} n_{f_1} n_{f_2} - 2v \frac{\partial u_2(x, y)}{\partial y} (n_{f_2})^2 - g\phi(x, y) = 0, \text{ on } \Gamma, \quad (22)$$

$$-2v \frac{\partial u_1(x, y)}{\partial x} n_{f_1} \tau_{i_1} - v \frac{\partial u_1(x, y)}{\partial y} n_{f_1} \tau_{i_2} - v \frac{\partial u_1(x, y)}{\partial y} n_{f_2} \tau_{i_1} - v \frac{\partial u_2(x, y)}{\partial x} n_{f_2} \tau_{i_1} - v \frac{\partial u_2(x, y)}{\partial x} n_{f_1} \tau_{i_2} \quad (23)$$

$$-2v \frac{\partial u_2(x, y)}{\partial y} n_{f_2} \tau_{i_2} - \frac{v\alpha\sqrt{d}}{\sqrt{\text{trace}(\Pi)}} u_1(x, y) \tau_{i_1} - \frac{v\alpha\sqrt{d}}{\sqrt{\text{trace}(\Pi)}} u_2(x, y) \tau_{i_2} = 0, \text{ on } \Gamma,$$

and the Dirichlet boundary condition:

$$\phi(x, y) = 0, \text{ on } \partial\Omega_p \setminus \Gamma, \quad (24)$$

$$u_1(x, y) = 0, \text{ on } \partial\Omega_f \setminus \Gamma, \quad (25)$$

$$u_2(x, y) = 0, \text{ on } \partial\Omega_f \setminus \Gamma, \quad (26)$$

$$\frac{\partial u_1(x, y)}{\partial x} + \frac{\partial u_2(x, y)}{\partial y} + p(x, y) = p(x, y), \text{ on } \partial\Omega_f, \quad (27)$$

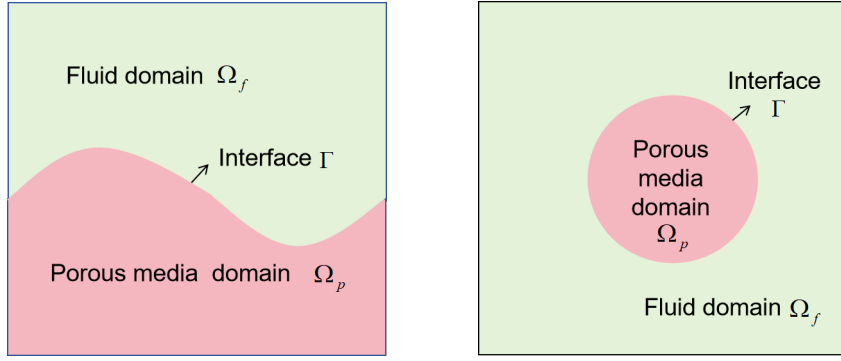


Figure 1: The distributions of the Stokes-Darcy coupled problem with unclosed interface(left) and closed interface(right).

3. Numerical Schemes

In this section, we briefly describe the numerical scheme of the GFDM, the Domain Decomposition scheme and the GFDM for the Stokes-Darcy coupled problem are provided to detailed describe the process of the numerical scheme.

3.1. The generalized finite difference method

For a given interior node (x_0, y_0) , we select m nearest nodes (x_k, y_k) ($k = 1, 2, \dots, m$) and make these $m + 1$ nodes form a star, as shown in Fig.2. Taking a 2D case for example, let $u_0 = u(x_0, y_0)$ is the function value at the node (x_0, y_0) and $u_k = u(x_k, y_k)$ ($k = 1, 2, \dots, m$) are function values at nodes (x_k, y_k) ($k = 1, 2, \dots, m$). To expand the values of $u_k = u(x_k, y_k)$ ($k = 1, 2, \dots, m$) around the given node (x_0, y_0) using the Taylor series:

$$u_k = u_0 + h_k \frac{\partial u_0}{\partial x} + l_k \frac{\partial u_0}{\partial y} + \frac{h_k^2}{2} \frac{\partial^2 u_0}{\partial x^2} + \frac{l_k^2}{2} \frac{\partial^2 u_0}{\partial y^2} + h_k l_k \frac{\partial^2 u_0}{\partial x \partial y} + O(\rho^3), k = 1, \dots, m, \quad (28)$$

where h_k and l_k are the distance between the node (x_k, y_k) and (x_0, y_0) :

$$h_k = x_k - x_0, k = 1, 2, \dots, m, \quad (29)$$

$$l_k = y_k - y_0, k = 1, 2, \dots, m. \quad (30)$$

$\frac{\partial u_0}{\partial x}, \frac{\partial u_0}{\partial y}, \frac{\partial^2 u_0}{\partial x^2}, \frac{\partial^2 u_0}{\partial y^2}, \frac{\partial^2 u_0}{\partial x \partial y}$ are partial derivatives of each order at the node (x_0, y_0) . By truncating the Taylor series expression (Eq.(28)) after the second order derivatives, a second order GFDM can be obtained, then a residual function $B_2(u)$ can be obtained,

$$B_2(u) = \sum_{k=1}^m [u_0 - u_k + h_k \frac{\partial u_0}{\partial x} + l_k \frac{\partial u_0}{\partial y} + \frac{h_k^2}{2} \frac{\partial^2 u_0}{\partial x^2} + \frac{l_k^2}{2} \frac{\partial^2 u_0}{\partial y^2} + h_k l_k \frac{\partial^2 u_0}{\partial x \partial y}] \omega_k, \quad (31)$$

in which ω_k ($k = 1, 2, \dots, m$) is the weighting coefficient at (x_k, y_k) . the weight function is taken as follows:

$$\omega_k = \begin{cases} 1 - 6(\frac{d_k}{d_m})^2 + 8(\frac{d_k}{d_m})^3 - 3(\frac{d_k}{d_m})^4, & d_k \leq d_m, \\ 0, & d_k \geq d_m. \end{cases} \quad (32)$$

Here $d_k = \sqrt{(x_k - x_0)^2 + (y_k - y_0)^2}$ is the distance between nodes (x_k, y_k) and (x_0, y_0) , and d_m is the maximum value of d_k ($k = 1, 2, \dots, m$). From the above weight function, we can see that the weighting coefficient is inversely proportional to the distance from the corresponding node (x_k, y_k) to (x_0, y_0) . To minimize the above residual function concerning the partial derivatives $D(u) = (\frac{\partial u_0}{\partial x}, \frac{\partial u_0}{\partial y}, \frac{\partial^2 u_0}{\partial x^2}, \frac{\partial^2 u_0}{\partial y^2}, \frac{\partial^2 u_0}{\partial x \partial y})^T$, that is, let

$$\frac{\partial B_2(u)}{\partial D_u} = 0, \quad (33)$$

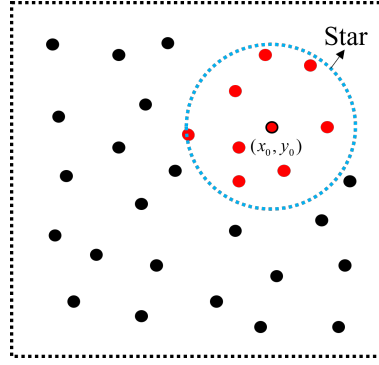


Figure 2: The star of a central node (x_0, y_0) for 2D case.

then the following linear equation system can be obtained,

$$AD_u = b, \quad (34)$$

where A is a symmetric matrix given by

$$A = \sum_{k=1}^m S_k^T S_k, \quad (35)$$

here S_k is a diagonal matrice. and its diagonal elements can be defined as

$$S_k = \omega_k(h_k, l_k, \frac{h_k^2}{2}, \frac{l_k^2}{2}, h_k l_k)^T, \quad (36)$$

and

$$b = BU = (-\sum_{k=1}^m \omega_k S_{(k)}, \omega_1 S_{(1)}, \omega_2 S_{(2)}, \dots, \omega_m S_{(m)})_{5 \times (m+1)} (u_0, u_1, \dots, u_m)^T, \quad (37)$$

in which $U = (u_0, u_1, \dots, u_m)^T$ are function values of all nodes inside the star. According to Eq. (34) and Eq. (37), the partial derivative vector D_u can be expressed as follows:

$$D_u = A^{-1}b = A^{-1}(BU) = (A^{-1}B)U = EU, \quad (38)$$

where

$$E = A^{-1}B, \quad (39)$$

is generally obtained by using the moving least-squares method. Based on the above analysis, the derivative at (x_0, y_0) can be expressed as a linear combination of the function values for itself and its m neighbouring nodes, as shown in Eq. (38). For example,

$$\frac{\partial^2 u_0}{\partial y^2} = \sum_{j=1}^m E_{4j} u_j^0. \quad (40)$$

It means that the second order derivative of the function value at the (x_0, y_0) can to be written as the product of the fourth row of the matrix formed by Eq. (39) and the matrix formed by the function values of the nodes inside the star. Repeating the same procedure for each node within the computational domain, we can obtain the algebraic equations for other interior points.

3.2. The handling skill for the Stokes-Darcy coupled problem

In this subsection, the idea of the Domain Decomposition is used to divide the transformed Stokes-Darcy coupled problem. By this scheme, the original Stokes/Darcy coupled problem (Eqs.(1),(3)-(9),(13),(16)) can be divided into two non-interface subproblems:

$$-\nabla \cdot T(\mathbf{u}_f, p_f) = \mathbf{f}_f, \quad \text{in } \Omega_f, \quad (41)$$

$$\Delta p = \nabla \cdot \mathbf{f}_f, \quad \text{in } \Omega_f, \quad (42)$$

$$\mathbf{u}_f = 0, \quad \text{on } \partial\Omega_f \setminus \Gamma, \quad (43)$$

$$\mathbf{u}_f + p(x, y) = p(x, y), \quad \text{on } \partial\Omega_f, \quad (44)$$

$$\nabla \cdot \mathbf{u}_f \cdot \mathbf{n}_f + \mathbf{u}_p \cdot \mathbf{n}_p = 0, \quad \text{on } \Gamma, \quad (45)$$

$$\mathbf{n}_f \cdot T(\mathbf{u}_f, p_f) \cdot \mathbf{n}_f = g\phi, \quad \text{on } \Gamma, \quad (46)$$

and

$$\mathbf{u}_p = -K\nabla\phi, \quad \text{in } \Omega_p, \quad (47)$$

$$\nabla \cdot \mathbf{u}_p = \mathbf{f}_p, \quad \text{in } \Omega_p, \quad (48)$$

$$\phi = 0, \quad \text{on } \partial\Omega_p \setminus \Gamma, \quad (49)$$

$$\mathbf{n}_f \cdot T(\mathbf{u}_f, p_f) \cdot \boldsymbol{\tau}_i = \frac{v\alpha\sqrt{d}}{\sqrt{\text{trace}(\Pi)}} \mathbf{u}_f \cdot \boldsymbol{\tau}_i, \quad 1 \leq i \leq d-1, \quad \text{on } \Gamma. \quad (50)$$

Due to the above problems are related to the matrix, these problems can be described by matrix components:

$$-2v \frac{\partial^2 u_1(x, y)}{\partial x^2} - v \frac{\partial^2 u_1(x, y)}{\partial y^2} - v \frac{\partial^2 u_2(x, y)}{\partial x \partial y} + \frac{\partial p(x, y)}{\partial x} = f_1(x, y), \quad \text{in } \Omega_f, \quad (51)$$

$$-v \frac{\partial^2 u_2(x, y)}{\partial x^2} - 2v \frac{\partial^2 u_2(x, y)}{\partial y^2} - v \frac{\partial^2 u_1(x, y)}{\partial x \partial y} + \frac{\partial p(x, y)}{\partial y} = f_2(x, y), \quad \text{in } \Omega_f, \quad (52)$$

$$\frac{\partial^2 p(x, y)}{\partial x^2} + \frac{\partial^2 p(x, y)}{\partial y^2} = 0, \quad \text{in } \Omega_f, \quad (53)$$

$$u_1(x, y) = 0, \quad \text{on } \partial\Omega_f \setminus \Gamma, \quad (54)$$

$$u_2(x, y) = 0, \quad \text{on } \partial\Omega_f \setminus \Gamma, \quad (55)$$

$$\frac{\partial u_1(x, y)}{\partial x} + \frac{\partial u_2(x, y)}{\partial y} + p(x, y) = p(x, y), \quad \text{on } \partial\Omega_f, \quad (56)$$

$$u_1(x, y)n_{f_1} + u_2(x, y)n_{f_2} - K \frac{\partial \phi(x, y)}{\partial x} n_{p_1} - K \frac{\partial \phi(x, y)}{\partial y} n_{p_2} = 0, \quad \text{on } \Gamma, \quad (57)$$

$$p(x, y) - 2v \frac{\partial u_1(x, y)}{\partial x} (n_{f_1})^2 - 2v \frac{\partial u_1(x, y)}{\partial y} n_{f_2} n_{f_1} - 2v \frac{\partial u_2(x, y)}{\partial x} n_{f_1} n_{f_2} - 2v \frac{\partial u_2(x, y)}{\partial y} (n_{f_2})^2 - g\phi(x, y) \quad (58)$$

$$= 0 \quad \text{on } \Gamma,$$

and

$$-K \frac{\partial^2 \phi(x, y)}{\partial x^2} - K \frac{\partial^2 \phi(x, y)}{\partial y^2} = f_p(x, y), \quad \text{in } \Omega_p, \quad (59)$$

$$\phi(x, y) = 0, \quad \text{on } \partial\Omega_p \setminus \Gamma, \quad (60)$$

$$-2v \frac{\partial u_1(x, y)}{\partial x} n_{f_1} \tau_{i_1} - v \frac{\partial u_1(x, y)}{\partial y} n_{f_1} \tau_{i_2} - v \frac{\partial u_1(x, y)}{\partial y} n_{f_2} \tau_{i_1} - v \frac{\partial u_2(x, y)}{\partial x} n_{f_2} \tau_{i_1} - v \frac{\partial u_2(x, y)}{\partial x} n_{f_1} \tau_{i_2} \quad (61)$$

$$-2v \frac{\partial u_2(x, y)}{\partial y} n_{f_2} \tau_{i_2} - \frac{v\alpha\sqrt{d}}{\sqrt{\text{trace}(\Pi)}} u_1(x, y) \tau_{i_1} - \frac{v\alpha\sqrt{d}}{\sqrt{\text{trace}(\Pi)}} u_2(x, y) \tau_{i_2} = 0, \quad \text{on } \Gamma,$$

From the above analysis, these subproblem (Eq.s(51)-(61)) are equivalent to the original interface problem (Eqs.(1),(3)-(9),(13),(16)).

3.3. The GFDM for the Stokes-Darcy coupled problem

In this part, we use the GFDM to analyze the Stokes-Darcy coupled problem Eqs.(51)-(61). Firstly, $N_{inp}^+ + N_{inp}^-$, $N_{bp}^+ + N_{bp}^-$ and $N_{\Gamma}^+ + N_{\Gamma}^-$ scattered nodes can be obtained by discretizing the computational domain $\Omega = \Omega^+ \cup \Omega^-$, the domain boundary $\partial\Omega = \partial\Omega^+ \cup \partial\Omega^-$ and the interface $\Gamma = \Gamma^+ \cup \Gamma^-$, respectively. In particular, the computational domain $\Omega = \Omega^+(t) \cup \Omega^-(t)$, the domain boundary $\partial\Omega(t) = \partial\Omega^+(t) \cup \partial\Omega^-(t)$ and the interface $\Gamma(t) = \Gamma^+(t) \cup \Gamma^-(t)$ are considered when the interface is moving. $\Gamma(t)$ is a sufficiently smooth closed curve. For simplicity, we assume that $\Gamma(t)$ does not touch the boundary. We assume that time t is a uniform distribution of points and discrete the time t with N_j^t nodes. That is let $dt = (T - 0)/N_j^t$ then $t = t_0 + (j - 1)dt$. If we fix on t , $t = t_j$, $\Gamma(t) = \Gamma_j$, the j_{th} location of the interface can be obtained. This means that we can get the exact interface information at t_j . Specially, the selection of interface points and the form of the star of the interface points can refer the article[36].

To enforce that the interior node satisfies the governing equation, the boundary node satisfies the boundary condition and the interface node satisfies the interface condition, $N_{inp}^+ + N_{inp}^- + N_{bp}^+ + N_{bp}^- + N_{\Gamma}^+ + N_{\Gamma}^-$ linear algebraic equations can be obtained. To solve this algebraic system of equations, the result can be obtained. For simplicity, the final system of linear equations can be rewritten in matrix form:

$$\hat{A}X = b, \quad (62)$$

where

$$\hat{A} = \left(\begin{array}{c|c} F & D_1 \\ \hline D_2 & D \end{array} \right), U = \left(\begin{array}{c} U^+ \\ U^- \end{array} \right), b = \left(\begin{array}{c} b^+ \\ b^- \end{array} \right), \quad (63)$$

Here

$$F = \left(\begin{array}{cc} G & P_1 \\ P_2 & P_p \end{array} \right), D_1 = \left(\begin{array}{c} D_{11} \\ D_{12} \\ D_{13} \end{array} \right), D_2 = \left(\begin{array}{ccc} D_{21} & D_{22} & D_{23} \end{array} \right), U^+ = \left(\begin{array}{c} U_1^+ \\ U_2^+ \\ P \end{array} \right), b^+ = \left(\begin{array}{c} b_1^+ \\ b_2^+ \\ b_3^+ \end{array} \right), \quad (64)$$

where

$$G = \left(\begin{array}{cc} G_{11} & G_{12} \\ G_{21} & G_{22} \end{array} \right), P_1 = \left(\begin{array}{c} P_{11} \\ P_{12} \end{array} \right), P_2 = \left(\begin{array}{cc} P_{21} & P_{22} \end{array} \right), \quad (65)$$

$$U_1^+ = (u_{1,1}^+, \dots, u_{1,N_{bp}^+}^+, u_{1,N_{bp}^++1}^+, \dots, u_{1,N_{bp}^++N_{\Gamma}^+}^+, u_{1,N_{bp}^++N_{\Gamma}^++1}^+, \dots, u_{1,N_{bp}^++N_{\Gamma}^++N_{inp}^+}^+)^T, \quad (66)$$

$$U_2^+ = (u_{2,1}^+, \dots, u_{2,N_{bp}^+}^+, u_{2,N_{bp}^++1}^+, \dots, u_{2,N_{bp}^++N_{\Gamma}^+}^+, u_{2,N_{bp}^++N_{\Gamma}^++1}^+, \dots, u_{2,N_{bp}^++N_{\Gamma}^++N_{inp}^+}^+)^T, \quad (67)$$

$$P = (p_1, \dots, p_{N_{bp}^+}, p_{N_{bp}^++1}, \dots, p_{N_{bp}^++N_{\Gamma}^+}, p_{N_{bp}^++N_{\Gamma}^++1}, \dots, p_{N_{bp}^++N_{\Gamma}^++N_{inp}^+})^T, \quad (68)$$

$$U^- = (\phi_1, \dots, \phi_{N_{bp}^-}, \phi_{N_{bp}^-+1}, \dots, \phi_{N_{bp}^-+N_{\Gamma}^-}, \phi_{N_{bp}^-+N_{\Gamma}^-+1}, \dots, \phi_{N_{bp}^-+N_{\Gamma}^-+N_{inp}^-})^T, \quad (69)$$

$$b_1^+ = (0, \dots, 0, 0, \dots, 0, f_{1,N_{bp}^++N_{\Gamma}^++1}, \dots, f_{1,N_{bp}^++N_{\Gamma}^++N_{inp}^+})^T, \quad (70)$$

$$b_2^+ = (0, \dots, 0, 0, \dots, 0, f_{2,N_{bp}^+ + N_\Gamma^+ + 1}, \dots, f_{2,N_{bp}^+ + N_\Gamma^+ + N_{inp}^+})^T, \quad (71)$$

$$b_3^+ = (p_1, \dots, p_{N_{bp}^+}, p_{N_{bp}^+ + 1}, \dots, p_{N_{bp}^+ + N_\Gamma^+}, 0, \dots, 0)^T, \quad (72)$$

$$b^- = (0, \dots, 0, 0, \dots, 0, f_{p,N_{bp}^- + N_\Gamma^- + 1}, \dots, f_{p,N_{bp}^- + N_\Gamma^- + N_{inp}^-})^T, \quad (73)$$

and

$$G_{11} = \begin{pmatrix} E_{N_{bp}^+ \times N_{bp}^+} & 0 & 0 \\ 0 & K_{1,N_\Gamma^+ \times N_\Gamma^+} & 0 \\ 0 & 0 & I_{1,N_{inp}^+ \times N_{inp}^+} \end{pmatrix}, G_{12} = \begin{pmatrix} 0 & 0 & 0 \\ 0 & K_{2,N_\Gamma^+ \times N_\Gamma^+} & 0 \\ 0 & 0 & I_{2,N_{inp}^+ \times N_{inp}^+} \end{pmatrix}, \quad (74)$$

$$G_{21} = \begin{pmatrix} 0 & 0 & 0 \\ 0 & K_{3,N_\Gamma^+ \times N_\Gamma^+} & 0 \\ 0 & 0 & I_{3,N_{inp}^+ \times N_{inp}^+} \end{pmatrix}, G_{22} = \begin{pmatrix} E_{N_{bp}^+ \times N_{bp}^+} & 0 & 0 \\ 0 & K_{4,N_\Gamma^+ \times N_\Gamma^+} & 0 \\ 0 & 0 & I_{4,N_{inp}^+ \times N_{inp}^+} \end{pmatrix}, \quad (75)$$

$$P_{11} = \begin{pmatrix} L_{1,N_{bp}^+ \times N_{bp}^+} & 0 & 0 \\ 0 & L_{2,N_\Gamma^+ \times N_\Gamma^+} & 0 \\ 0 & 0 & 0 \end{pmatrix}, P_{12} = \begin{pmatrix} L_{3,N_{bp}^+ \times N_{bp}^+} & 0 & 0 \\ 0 & L_{4,N_\Gamma^+ \times N_\Gamma^+} & 0 \\ 0 & 0 & 0 \end{pmatrix}, \quad (76)$$

$$P_{21} = \begin{pmatrix} 0 & 0 & 0 \\ 0 & 0 & 0 \\ 0 & 0 & R_{1,N_{inp}^+ \times N_{inp}^+} \end{pmatrix}, P_{22} = \begin{pmatrix} 0 & 0 & 0 \\ 0 & E_{N_\Gamma^+ \times N_\Gamma^+} & 0 \\ 0 & 0 & R_{2,N_{inp}^+ \times N_{inp}^+} \end{pmatrix}, \quad (77)$$

$$P_p = \begin{pmatrix} E_{N_{bp}^+ \times N_{bp}^+} & 0 & 0 \\ 0 & E_{N_\Gamma^+ \times N_\Gamma^+} & 0 \\ 0 & 0 & P_{1,N_{inp}^+ \times N_{inp}^+} \end{pmatrix}, \quad (78)$$

$$D_{11} = \begin{pmatrix} 0 & 0 & 0 \\ 0 & M_{1,N_\Gamma^- \times N_\Gamma^-} & 0 \\ 0 & 0 & 0 \end{pmatrix}, D_{12} = \begin{pmatrix} 0 & 0 & 0 \\ 0 & M_{2,N_\Gamma^- \times N_\Gamma^-} & 0 \\ 0 & 0 & 0 \end{pmatrix}, D_{13} = D_{23} = 0, \quad (79)$$

$$D_{21} = \begin{pmatrix} 0 & 0 & 0 \\ 0 & M_{3,N_\Gamma^- \times N_\Gamma^-} & 0 \\ 0 & 0 & 0 \end{pmatrix}, D_{22} = \begin{pmatrix} 0 & 0 & 0 \\ 0 & M_{4,N_\Gamma^- \times N_\Gamma^-} & 0 \\ 0 & 0 & 0 \end{pmatrix}, D = \begin{pmatrix} E_{N_{bp}^- \times N_{bp}^-} & 0 & 0 \\ 0 & 0 & 0 \\ 0 & 0 & M_{5,N_{inp}^- \times N_{inp}^-} \end{pmatrix}, \quad (80)$$

in which

$$K_{1,N_\Gamma^+ \times N_\Gamma^+}(i, j) = n_{f_1}, \quad (81)$$

$$K_{2,N_\Gamma^+ \times N_\Gamma^+}(i, j) = n_{f_2}, \quad (82)$$

$$K_{3,N_\Gamma^+ \times N_\Gamma^+}(i, j) = -2\nu E(1, i) n_{f_1}^2, \quad (83)$$

$$K_{4,N_{\Gamma}^{+} \times N_{\Gamma}^{+}}(i, j) = -2\nu E(1, i) n_{f_1} n_{f_2}, \quad (84)$$

$$I_{1,N_{inp}^{+} \times N_{inp}^{+}}(i, j) = -2\nu E(3, i) - \nu E(4, i), \quad (85)$$

$$I_{2,N_{inp}^{+} \times N_{inp}^{+}}(i, j) = -\nu E(5, i), \quad (86)$$

$$I_{3,N_{inp}^{+} \times N_{inp}^{+}}(i, j) = -\nu E(5, i), \quad (87)$$

$$I_{4,N_{inp}^{+} \times N_{inp}^{+}}(i, j) = -\nu E(3, i) - 2\nu E(4, i), \quad (88)$$

$$L_{1,N_{bp}^{+} \times N_{bp}^{+}}(i, j) = E(1, i), \quad (89)$$

$$L_{3,N_{bp}^{+} \times N_{bp}^{+}}(i, j) = E(2, i), \quad (90)$$

$$L_{2,N_{\Gamma}^{+} \times N_{\Gamma}^{+}}(i, j) = E(1, i), \quad (91)$$

$$L_{4,N_{\Gamma}^{+} \times N_{\Gamma}^{+}}(i, j) = E(2, i), \quad (92)$$

$$R_{1,N_{inp}^{+} \times N_{inp}^{+}}(i, j) = E(1, i), \quad (93)$$

$$R_{2,N_{inp}^{+} \times N_{inp}^{+}}(i, j) = E(2, i), \quad (94)$$

$$P_{1,N_{inp}^{+} \times N_{inp}^{+}}(i, j) = E(3, i) + E(4, i), \quad (95)$$

$$M_{1,N_{\Gamma}^{-} \times N_{\Gamma}^{-}}(i, j) = -2\nu E(1, i) n_{f_1} \tau_{i_1} - \nu E(2, i) n_{f_1} \tau_{i_2} - \nu E(2, i) n_{f_2} \tau_{i_1} - \frac{\nu \alpha \sqrt{d}}{\sqrt{\text{trace}(\Pi)}} \tau_{i_1}, \quad (96)$$

$$M_{2,N_{\Gamma}^{-} \times N_{\Gamma}^{-}}(i, j) = -\nu E(1, i) n_{f_2} \tau_{i_1} - \nu E(1, i) n_{f_1} \tau_{i_2} - 2\nu E(2, i) n_{f_2} \tau_{i_2} - \frac{\nu \alpha \sqrt{d}}{\sqrt{\text{trace}(\Pi)}} \tau_{i_2}, \quad (97)$$

$$M_{3,N_{\Gamma}^{-} \times N_{\Gamma}^{-}}(i, j) = -K E(1, i) n_{p_1} - K E(2, i) n_{p_2}, \quad (98)$$

$$M_{4,N_{\Gamma}^{-} \times N_{\Gamma}^{-}}(i, j) = -g, \quad (99)$$

$$M_{5,N_{inp}^{-} \times N_{inp}^{-}}(i, j) = -K E(3, i) - K E(4, i). \quad (100)$$

The matrices \hat{A} is formed according to the idea of the domain decomposition, F and D are formed by the governing equations (Eq.(51)-(53),Eq.(59)), the Dirichlet boundary conditions (Eq.(54)-(56),Eq.(60)) and the interface condition (Eq.(57)-(58),Eq.(61)), respectively. The interface parts of F , D_1 , D_2 , D are all created by the interface condition (Eq.(57),Eq.(58),Eq.(61)). Obviously, it is simple to use the above matrices to describe the interface conditions and the interface informations are only used on the interface points, the GFDM has advantage in dealing with the complex interface and the moving interface. P_1, P_2 obtain the pressure information in Eq.(51)-(52). P_p is formed according to the governing equation (Eq.(53)). we can obtain different matrix if we use different form which is used to enrich the information about the pressure p . We can see that the matrix \hat{A} is sparse.

4. Convergence analysis

Theorem 1: The even $(2i)$ -order generalized finite difference method has an even $(2i)$ -order convergence order, in which $i \in \mathbb{Z}^{+}$.

Proof:

For $i = 1$, we consider the fourth order Taylor series expanding, the residual function can be obtained

$$B_2^*(u) = \sum_{k=1}^m [(u_0 - u_k + h_k \frac{\partial u_0}{\partial x} + l_k \frac{\partial u_0}{\partial y} + \frac{h_k^2}{2} \frac{\partial^2 u_0}{\partial x^2} + \frac{l_k^2}{2} \frac{\partial^2 u_0}{\partial y^2} + h_k l_k \frac{\partial^2 u_0}{\partial x \partial y} + \frac{1}{6} (h_k \frac{\partial u_0}{\partial x} + l_k \frac{\partial u_0}{\partial y})^3 + \frac{1}{24} (h_k \frac{\partial u_0}{\partial x} + l_k \frac{\partial u_0}{\partial y})^4 + \dots] \omega_k]^2, \quad (101)$$

Regarding the second-order partial derivative $D_{2,u}$, minimizing the extended residual function $B^*(u)$

$$\frac{\partial B_2^*(u)}{\partial D_{2,u}} = 0, \quad (102)$$

then the following linear equation system can be obtained,

$$AD_{2,u} = b_2^*, \quad (103)$$

$$b_2^* = b_2 - b_2^{**}, \quad (104)$$

$$b_2^{**} = \begin{pmatrix} \sum_{k=1}^m [\frac{h_k}{6} (h_k \frac{\partial u_0}{\partial x} + l_k \frac{\partial u_0}{\partial y})^3 \omega_k^2 + \frac{h_k}{24} (h_k \frac{\partial u_0}{\partial x} + l_k \frac{\partial u_0}{\partial y})^4 \omega_k^2 + \dots] \\ \sum_{k=1}^m [\frac{l_k}{6} (h_k \frac{\partial u_0}{\partial x} + l_k \frac{\partial u_0}{\partial y})^3 \omega_k^2 + \frac{l_k}{24} (h_k \frac{\partial u_0}{\partial x} + l_k \frac{\partial u_0}{\partial y})^4 \omega_k^2 + \dots] \\ \dots \\ \sum_{k=1}^m [\frac{h_k l_k}{6} (h_k \frac{\partial u_0}{\partial x} + l_k \frac{\partial u_0}{\partial y})^3 \omega_k^2 + \frac{h_k l_k}{24} (h_k \frac{\partial u_0}{\partial x} + l_k \frac{\partial u_0}{\partial y})^4 \omega_k^2 + \dots] \end{pmatrix}. \quad (105)$$

To define the following function

$$f_2(u) = (\beta, \beta, \dots, \beta)_{1 \times 5} D_{2,u} = (\beta, \beta, \dots, \beta)_{1 \times 5} A^{-1} b_2 - (\beta, \beta, \dots, \beta)_{1 \times 5} A^{-1} b_2^{**} \quad (106)$$

According to the explicit form of the generalized finite difference method(From Ref[44]),

$$f_2(u) = -m_0 + \sum_{k=1}^m m_k u_k \quad (107)$$

in which

$$u_0 = \frac{1}{m_0} \sum_{k=1}^m m_k u_k, \quad \sum_{k=1}^m m_k = m_0. \quad (108)$$

then

$$f_2(u) - (\beta, \beta, \dots, \beta)_{1 \times 5} D_{2,u} = -(\beta, \beta, \dots, \beta)_{1 \times 5} A^{-1} b_2^{**} = \varepsilon_{2s}. \quad (109)$$

Similaring to equation (108) and (109) in reference[44], and let $m_k = \frac{\mu_k}{h_k^2 + l_k^2}$, $\mu_k \in \mathbf{R}$, in which the definition of m_k can be seen in Appendix A, then

$$\begin{aligned} \varepsilon_{2s} &= -(\beta, \beta, \dots, \beta)_{1 \times 5} A^{-1} \begin{pmatrix} \sum_{k=1}^m [\frac{1}{6} (h_k \frac{\partial u_0}{\partial x} + l_k \frac{\partial u_0}{\partial y})^3 \omega_k^2 h_k + \frac{1}{24} (h_k \frac{\partial u_0}{\partial x} + l_k \frac{\partial u_0}{\partial y})^4 \omega_k^2 h_k + \dots] \\ \sum_{k=1}^m [\frac{1}{6} (h_k \frac{\partial u_0}{\partial x} + l_k \frac{\partial u_0}{\partial y})^3 \omega_k^2 l_k + \frac{1}{24} (h_k \frac{\partial u_0}{\partial x} + l_k \frac{\partial u_0}{\partial y})^4 \omega_k^2 l_k + \dots] \\ \dots \\ \sum_{k=1}^m [\frac{1}{6} (h_k \frac{\partial u_0}{\partial x} + l_k \frac{\partial u_0}{\partial y})^3 \omega_k^2 h_k l_k + \frac{1}{24} (h_k \frac{\partial u_0}{\partial x} + l_k \frac{\partial u_0}{\partial y})^4 \omega_k^2 h_k l_k + \dots] \end{pmatrix} \\ &= -\sum_{k=1}^m \mu_k [\frac{1}{6(h_k^2 + l_k^2)} (h_k \frac{\partial u_0}{\partial x} + l_k \frac{\partial u_0}{\partial y})^3 + \frac{1}{24(h_k^2 + l_k^2)} (h_k \frac{\partial u_0}{\partial x} + l_k \frac{\partial u_0}{\partial y})^4] + o(h_k^3, l_k^3). \end{aligned} \quad (110)$$

Therefore, the conclusion can be obtained when $i = 1$. It means that the second order generalized finite difference method has an second order convergence order.

For $i = 2$, we consider the sixth order Taylor series expanding, the residual function can be obtained

$$\begin{aligned} B_4^*(u) &= \sum_{k=1}^m [(u_0 - u_k + h_k \frac{\partial u_0}{\partial x} + l_k \frac{\partial u_0}{\partial y} + \frac{h_k^2}{2} \frac{\partial^2 u_0}{\partial x^2} + \frac{l_k^2}{2} \frac{\partial^2 u_0}{\partial y^2} + h_k l_k \frac{\partial^2 u_0}{\partial x \partial y} + \frac{h_k^3}{6} \frac{\partial^3 u_0}{\partial x^3} + \frac{l_k^3}{6} \frac{\partial^3 u_0}{\partial y^3} \\ &\quad + \frac{h_k^2 l_k}{2} \frac{\partial^3 u_0}{\partial x^2 \partial y} + \frac{h_k l_k^2}{2} \frac{\partial^3 u_0}{\partial x \partial y^2} + \frac{h_k^4}{24} \frac{\partial^4 u_0}{\partial x^4} + \frac{l_k^4}{24} \frac{\partial^4 u_0}{\partial y^4} + \frac{h_k^3 l_k}{6} \frac{\partial^4 u_0}{\partial x^3 \partial y} + \frac{h_k^2 l_k^2}{4} \frac{\partial^4 u_0}{\partial x^2 \partial y^2} + \frac{l_k^3 h_k}{6} \frac{\partial^4 u_0}{\partial x \partial y^3} \\ &\quad + \frac{1}{120} (h_k \frac{\partial u_0}{\partial x} + l_k \frac{\partial u_0}{\partial y})^5 + \frac{1}{720} (h_k \frac{\partial u_0}{\partial x} + l_k \frac{\partial u_0}{\partial y})^6 \omega_k + \dots]^2 \end{aligned} \quad (111)$$

Regarding the fourth order partial derivative $D_4(u) = (\frac{\partial u_0}{\partial x}, \frac{\partial u_0}{\partial y}, \frac{\partial^2 u_0}{\partial x^2}, \frac{\partial^2 u_0}{\partial y^2}, \frac{\partial^2 u_0}{\partial x \partial y}, \frac{\partial^3 u_0}{\partial x^3}, \frac{\partial^3 u_0}{\partial y^3}, \frac{\partial^3 u_0}{\partial x^2 \partial y}, \frac{\partial^3 u_0}{\partial x \partial y^2}, \frac{\partial^4 u_0}{\partial x^4}, \frac{\partial^4 u_0}{\partial y^4}, \frac{\partial^4 u_0}{\partial x^3 \partial y}, \frac{\partial^4 u_0}{\partial x^2 \partial y^2}, \frac{\partial^4 u_0}{\partial x \partial y^3})^T$, minimizing the extended residual function $B_4^*(u)$

$$\frac{\partial B_4^*(u)}{\partial D_{4,u}} = 0, \quad (112)$$

then the following linear equation system can be obtained,

$$AD_{4,u} = b^*, \quad (113)$$

$$b_4^* = b_4 - b_4^{**}, \quad (114)$$

in which

$$b_4^{**} = \begin{pmatrix} \sum_{k=1}^m [\frac{1}{120}(h_k \frac{\partial u_0}{\partial x} + l_k \frac{\partial u_0}{\partial y})^5 \omega_k^2 h_k + \frac{1}{720}(h_k \frac{\partial u_0}{\partial x} + l_k \frac{\partial u_0}{\partial y})^6 \omega_k^2 h_k + \dots] \\ \sum_{k=1}^m [\frac{1}{120}(h_k \frac{\partial u_0}{\partial x} + l_k \frac{\partial u_0}{\partial y})^5 \omega_k^2 l_k + \frac{1}{720}(h_k \frac{\partial u_0}{\partial x} + l_k \frac{\partial u_0}{\partial y})^6 \omega_k^2 l_k + \dots] \\ \dots \\ \sum_{k=1}^m [\frac{1}{120}(h_k \frac{\partial u_0}{\partial x} + l_k \frac{\partial u_0}{\partial y})^5 \omega_k^2 h_k l_k^3 + \frac{1}{720}(h_k \frac{\partial u_0}{\partial x} + l_k \frac{\partial u_0}{\partial y})^6 \omega_k^2 h_k l_k^3 + \dots] \end{pmatrix} \quad (115)$$

Therefore,

$$\varepsilon_{4s} = -(\beta, \beta, \dots, \beta)_{1 \times 14} A^{-1} b^{**} \quad (116)$$

It is similar to the process at $i = 1$, let $m_k = \frac{\mu_k}{h_k^2 + l_k^2}$, $\mu_k \in R$, in which the definition of m_k is similar to Appendix A, and then

$$\varepsilon_{4s} = - \sum_{k=1}^m m_k [\frac{1}{120(h_k^2 + l_k^2)} (h_k \frac{\partial u_0}{\partial x} + l_k \frac{\partial u_0}{\partial y})^5 + \frac{1}{720(h_k^2 + l_k^2)} (h_k \frac{\partial u_0}{\partial x} + l_k \frac{\partial u_0}{\partial y})^6] + o(h_k^5, l_k^5). \quad (117)$$

Therefore, the conclusion can be obtained when $i = 2$. It means that the fourth order generalized finite difference method has an fourth order convergence order. and so forth...

To suppose the conclusion can be obtained when $i = n - 1$

$$\varepsilon_{(2n-2)s} = -(\beta, \beta, \dots, \beta)_{1 \times N_{Partial}} A^{-1} b^{**} \quad (118)$$

let $m_k = \frac{\mu_k}{h_k^2 + l_k^2}$, $\mu_k \in R$, in which the definition of m_k is similar to Appendix A, and then

$$\varepsilon_{(2n-2)s} = - \sum_{k=1}^m [\frac{1}{(2n-1)!} (h_k \frac{\partial u_0}{\partial x} + l_k \frac{\partial u_0}{\partial y})^{2n-1} + \frac{1}{(2n)!} (h_k \frac{\partial u_0}{\partial x} + l_k \frac{\partial u_0}{\partial y})^{2n}] + o(h_k^{2n-1}, l_k^{2n-1}). \quad (119)$$

To truncate the terms of the Taylor series after $2n+2$ orders when $i = n$, construct an extended residual function, and minimize the extended residual function, the error can be obtained:

$$\varepsilon_{2ns} = -(\beta, \beta, \dots, \beta)_{1 \times N_{Partial}} A^{-1} \begin{pmatrix} \sum_{k=1}^m [\frac{1}{(2n+1)!} (h_k \frac{\partial u_0}{\partial x} + l_k \frac{\partial u_0}{\partial y})^{2n+1} \omega_k^2 h_k + \frac{1}{(2n+2)!} (h_k \frac{\partial u_0}{\partial x} + l_k \frac{\partial u_0}{\partial y})^{2n+2} \omega_k^2 h_k + \dots] \\ \sum_{k=1}^m [\frac{1}{(2n+1)!} (h_k \frac{\partial u_0}{\partial x} + l_k \frac{\partial u_0}{\partial y})^{2n+1} \omega_k^2 l_k + \frac{1}{(2n+2)!} (h_k \frac{\partial u_0}{\partial x} + l_k \frac{\partial u_0}{\partial y})^{2n+2} \omega_k^2 l_k + \dots] \\ \dots \\ \sum_{k=1}^m [\frac{1}{(2n+1)!} (h_k \frac{\partial u_0}{\partial x} + l_k \frac{\partial u_0}{\partial y})^{2n+1} \omega_k^2 h_k l_k^{(2n-1)} + \frac{1}{(2n+2)!} (h_k \frac{\partial u_0}{\partial x} + l_k \frac{\partial u_0}{\partial y})^{2n+2} \omega_k^2 h_k l_k^{(2n-1)} + \dots] \end{pmatrix} \quad (120)$$

let $m_k = \frac{\mu_k}{h_k^2 + l_k^2}$, $\mu_k \in R$, in which the definition of m_k is similar to Appendix A, and then

$$\varepsilon_{2ns} = - \sum_{k=1}^m [\frac{1}{(2n+1)!} (h_k \frac{\partial u_0}{\partial x} + l_k \frac{\partial u_0}{\partial y})^{2n+1} + \frac{1}{(2n+2)!} (h_k \frac{\partial u_0}{\partial x} + l_k \frac{\partial u_0}{\partial y})^{2n+2}] + o(h_k^{2n+1}, l_k^{2n+1}). \quad (121)$$

Therefore, the conclusion can be obtained when $i = n$. It means that the 2nth-order generalized finite difference method has an 2nth-order convergence order. In which, $N_{Partial}$ denotes the total number of partial derivatives of the corresponding order.

According to mathematical induction, the above conclusion holds true, the 2ith-order generalized finite difference method has an 2ith-order convergence order, in which $i \in \mathbb{Z}^+$.

5. Numerical simulations

In this section, four examples are provided to show the accuracy, stability and high efficiency of the meshless GFDM for solving the Stokes-Darcy coupled problem with the linear interface in Example 1-Example 2, the closed complex interface in Example 3 and the moving interface in Example 4. In Example 1, we use the fixed kinematic viscosity ν of the fluid and the element of the hydraulic conductivity tensor K . In Example 2, the varying physical coefficients ν and K are used.

For simplicity, we defined the error norms as follows:

$$L_\infty = \max |u_i - u(x_i)| (i = 1, 2, \dots, N_T), \quad (122)$$

$$L_2 = \left[\sum_{i=1}^{N_T} \frac{(u_i - u(x_i))^2}{N_T} \right]^{\frac{1}{2}} (i = 1, 2, \dots, N_T), \quad (123)$$

$$H^1 = \left[\sum_{i=1}^{N_T} \frac{(\nabla u_i - \nabla u(x_i))^2}{N_T} \right]^{\frac{1}{2}} (i = 1, 2, \dots, N_T). \quad (124)$$

and the relative errors are defined as follows

$$L_{\infty, relative} = \frac{\max |u_i - u(x_i)|}{\max |u(x_i)|} (i = 1, 2, \dots, N_T), \quad (125)$$

$$L_{2, relative} = \frac{\left[\sum_{i=1}^{N_T} \frac{(u_i - u(x_i))^2}{N_T} \right]^{\frac{1}{2}}}{\left[\sum_{i=1}^{N_T} \frac{u(x_i)^2}{N_T} \right]^{\frac{1}{2}}} (i = 1, 2, \dots, N_T), \quad (126)$$

$$H_{relative}^1 = \frac{\left[\sum_{i=1}^{N_T} \frac{(\nabla u_i - \nabla u(x_i))^2}{N_T} \right]^{\frac{1}{2}}}{\left[\sum_{i=1}^{N_T} \frac{(\nabla u(x_i))^2}{N_T} \right]^{\frac{1}{2}}} (i = 1, 2, \dots, N_T). \quad (127)$$

Note that the H^1 and $H_{relative}^1$ of the velocity of Darcy \mathbf{u}_p contains the first and second order derivatives of ϕ , which can deduce that the numerical errors can illustrate the advantage of the GFDM for the derivative functions. u_i and $u(x_i)$ are the numerical and exact solution at point x_i , respectively. Let the domain Ω is a rectangle, Ω_f is the upper domain and Ω_p is the lower domain for linear interface Γ . Ω_f outside the interface Γ and $\Omega_p = \Omega / (\Omega_f \cup \Gamma)$ inside closed interface Γ . N_T is the number of all scattered nodes in Ω_f , Ω_p , $\partial\Omega_f$, $\partial\Omega_p$ and Γ . Namely, $N_T = N_{f,inp} + N_{p,inp} + N_{f,bp} + N_{p,bp} + N_{f,\Gamma} + N_{p,\Gamma}$. For convenience, we set $\mathbf{K} = \mathbf{KI}$, where K is a positive constant. The global domain Ω consists of two subdomains with free fluid flow region Ω_f and porous medium region Ω_p , where the interface between the conduit and matrix region is Γ and $\Omega = \Omega_f \cup \Omega_p \cup \Gamma$.

5.1. Example 1: The Stokes-Darcy coupled problem with a fixed physical coefficients

In this example, we consider the Stokes-Darcy coupled problem with a linear interface (see Fig.3). The exact solution are

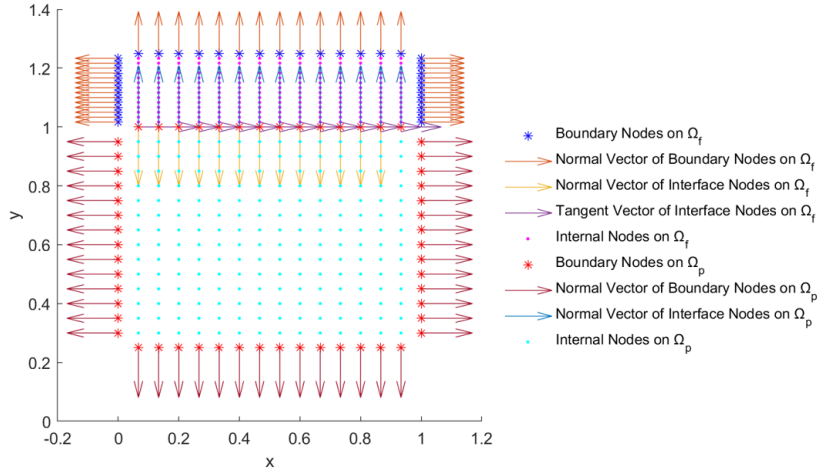


Figure 3: The point collocation for Example 1 Case 1.

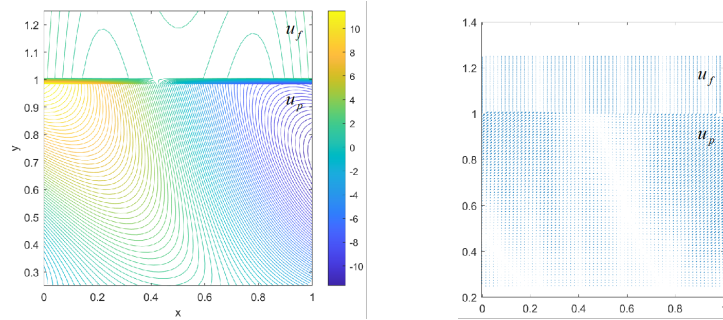


Figure 4: The contour (left) and the vector (right) of the numerical solution for Example 1 Case 1.

$$\mathbf{u}_f = (u_1, u_2)^T = \begin{pmatrix} [x^2(y-1)^2 + y] \\ [-\frac{2}{3}x(y-1)^3 + [2 - \pi \sin(\pi x)]] \end{pmatrix},$$

$$p = [2 - \pi \sin(\pi x)] \sin(\frac{1}{2}\pi y),$$

$$\phi = [2 - \pi \sin(\pi x)][1 - y - \cos(\pi y)],$$

$$\mathbf{u}_p = -K \nabla \phi.$$

The fixed kinematic viscosity $\nu = 1$ of fluid and the element of hydraulic conductivity tensor $K = 1$.

Case 1: $\phi = 0$, on Γ_p , $\Omega_f = [0, 1] \times [1, 1.25]$, $\Omega_p = [0, 1] \times [0.25, 1]$, $\Gamma = (0, 1) \times [1]$, $\frac{av\sqrt{d}}{\sqrt{\text{trace}(\Pi)}} = 1$, $g = 1$.

Case 2: $\mathbf{u}_p \cdot \mathbf{n}_p = 0$, on Γ_p , $\Omega_f = [0, 1] \times [1, 2]$, $\Omega_p = [0, 1] \times [0, 1]$, $\Gamma = (0, 1) \times [1]$, $\alpha = 1$, $g = 1$.

Fig.3 and Fig. 5 present the point collocations, in which we can see that the point collocation in each subdomain and the distributions of the normal vector and tangent vector for both Case 1 and Case 2. The contour (left) and the vector (right) of the numerical solution are shown in Fig.4 and Fig. 6, we can see that the distributions of the numerical solutions. The comparison between the GFDM and the LGI FEM[23] is given in Table. 1. The comparison between the GFDM and the FEDDM[20] is given in Table. 4. From these tables, we can see that our method is more accurate than the LGI FEM[23] and FEDDM [20]highly efficient because the CPU time is very small. Furthermore, our errors are all relative errors which can illustrate the numerical solution are accurate and stable. Table.2 and Table.3 show the $L_2, H^1_{relative}$ errors when the 2nd GFDM, 4th GFDM and 6th GFDM are adopted. Table.5 and Table.6 show the

Table 1

The comparison between the GFDM and the LGI FEM [23] for Example 1 Case 1

	N_x	h	u_f	p	ϕ	$CPU(s)$
			$L_{2,relative}$	$H^1_{relative}$	$L_{2,relative}$	$H^1_{relative}$
2nd GFDM $m = 40$	8		8.00×10^{-2}	2.77×10^{-1}	2.23×10^{-1}	7.36×10^{-1}
	16		1.58×10^{-3}	2.03×10^{-2}	8.32×10^{-3}	1.63×10^{-2}
	32		4.30×10^{-4}	4.61×10^{-3}	2.30×10^{-3}	4.92×10^{-3}
	64		1.10×10^{-4}	1.09×10^{-3}	5.92×10^{-4}	1.31×10^{-3}
	128		2.77×10^{-5}	2.65×10^{-4}	1.48×10^{-4}	3.35×10^{-4}
	Order		2.71	3.08	2.64	1.94
LGI FEM[23]		$\frac{1}{8}$	1.55×10^{-2}	3.97×10^{-1}	1.15×10^{-1}	1.14×10^{-2}
		$\frac{1}{16}$	3.92×10^{-3}	1.98×10^{-1}	3.67×10^{-2}	2.88×10^{-3}
		$\frac{1}{32}$	9.87×10^{-4}	9.91×10^{-2}	1.16×10^{-2}	7.20×10^{-4}
		$\frac{1}{64}$	2.47×10^{-4}	4.95×10^{-2}	3.71×10^{-3}	1.80×10^{-4}
		$\frac{1}{128}$	6.20×10^{-5}	2.48×10^{-2}	1.22×10^{-3}	4.50×10^{-5}
	Order		1.99	1.00	1.64	2.00

Table 2

The $L_{2,relative}$ errors when the different order GFDMs are adopted for Example 1 Case 1

	N_x	u_f	p		ϕ		u_p		$CPU(s)$	
		$L_{2,relative}$	Order	$L_{2,relative}$	Order	$L_{2,relative}$	Order	$L_{2,relative}$	Order	
2nd order GFDM $m = 40$	16	1.58×10^{-3}	—	8.32×10^{-3}	—	1.60×10^{-2}	—	1.28×10^{-2}	—	0.13
	32	4.30×10^{-4}	1.88	2.30×10^{-3}	1.85	4.92×10^{-3}	1.70	2.44×10^{-3}	2.39	0.27
	64	1.10×10^{-4}	1.97	5.92×10^{-4}	1.96	1.31×10^{-3}	1.91	5.33×10^{-4}	2.19	0.89
	128	2.77×10^{-5}	1.99	1.48×10^{-4}	2.00	3.35×10^{-4}	1.97	1.25×10^{-4}	2.09	4.14
4th order GFDM $m = 210$	32	2.74×10^{-5}	—	1.32×10^{-4}	—	2.87×10^{-4}	—	2.48×10^{-4}	—	1.23
	64	1.34×10^{-6}	4.35	8.50×10^{-6}	3.96	2.05×10^{-5}	3.81	1.07×10^{-5}	4.53	66.2
	128	8.86×10^{-8}	3.92	5.75×10^{-7}	3.89	1.40×10^{-6}	3.88	5.06×10^{-7}	4.40	47.1
6th order GFDM $m = 450$	32	1.63×10^{-6}	—	1.11×10^{-5}	—	2.53×10^{-5}	—	1.79×10^{-5}	—	5.06
	64	3.05×10^{-8}	5.74	2.06×10^{-7}	5.74	4.16×10^{-7}	5.92	2.33×10^{-7}	6.26	88.6
	128	5.40×10^{-10}	5.82	3.70×10^{-9}	5.80	7.24×10^{-9}	5.85	3.16×10^{-9}	6.21	183.2

Table 3

The $H^1_{relative}$ errors when the different order GFDMs are adopted for Example 1 Case 1

	N_x	u_f		p		ϕ		u_p		$CPU(s)$
		$H^1_{relative}$	Order	$H^1_{relative}$	Order	$H^1_{relative}$	Order	$H^1_{relative}$	Order	
2nd order GFDM $m = 40$	8	2.77×10^{-1}	—	3.43×10^{-1}	—	1.11×10^{-1}	—	3.86×10^{-1}	—	0.17
	16	2.03×10^{-2}	3.78	1.84×10^{-2}	4.22	1.63×10^{-2}	2.77	1.14×10^{-1}	1.76	0.14
	32	4.61×10^{-3}	2.13	4.88×10^{-3}	1.92	2.78×10^{-3}	2.55	3.70×10^{-2}	1.63	0.28
	64	1.09×10^{-3}	2.08	1.30×10^{-3}	1.91	5.61×10^{-4}	2.31	1.25×10^{-2}	1.57	0.91
	128	2.65×10^{-4}	2.04	3.52×10^{-4}	1.89	1.27×10^{-4}	2.14	4.31×10^{-3}	1.53	4.22
4th order GFDM $m = 210$	32	1.80×10^{-4}	—	3.27×10^{-4}	—	2.56×10^{-4}	—	2.04×10^{-3}	—	1.27
	64	6.23×10^{-6}	4.85	1.96×10^{-5}	4.06	1.08×10^{-5}	4.56	1.75×10^{-4}	3.55	65.5
	128	2.68×10^{-7}	4.54	1.20×10^{-6}	4.03	5.09×10^{-7}	4.41	1.49×10^{-5}	3.56	45.6
6th order GFDM $m = 450$	32	3.79×10^{-6}	—	8.18×10^{-6}	—	1.80×10^{-5}	—	1.41×10^{-4}	—	5.17
	64	7.27×10^{-8}	5.70	1.12×10^{-7}	6.19	2.37×10^{-7}	6.25	3.60×10^{-6}	5.29	79.8
	128	1.23×10^{-9}	5.88	4.31×10^{-9}	4.70	3.18×10^{-9}	6.22	7.87×10^{-8}	5.52	171.3

$L_2, H^1_{relative}$ errors when the 4th GFDM and 6th GFDM are adopted. We can see that the 2nth order coverage can be obtained, when the 2nth order derivatives of Taylor series are truncated, (n=1,2,3).

5.2. Example 2: The Stokes-Darcy coupled problem with a varying physical coefficients

In this example, we consider the Stokes-Darcy coupled problem with a linear interface (see Fig.5). The exact solutions are

$$\mathbf{u}_f = (u_1, u_2)^T = \begin{pmatrix} [y^2 - 2y + 1] \\ [x^2 - x] \end{pmatrix},$$

$$p = 2v(x + y - 1) + \frac{1}{3K},$$

$$\phi = \frac{1}{K}[x(1-x)(y-1) + \frac{1}{3}y^3 - y^2 + y] + 2vx,$$

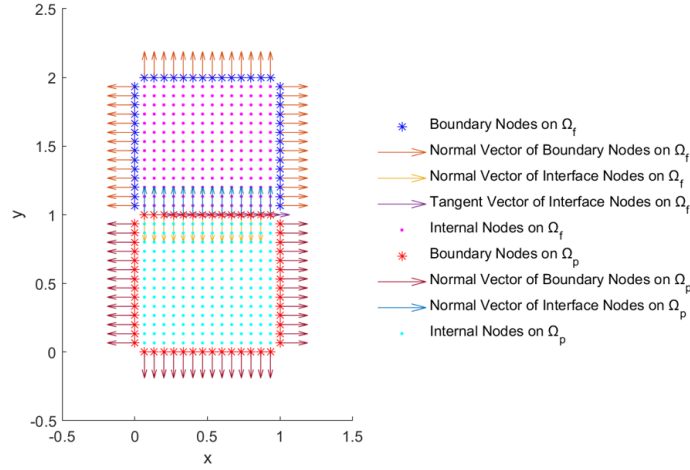


Figure 5: The point collocation for Example 1 Case 2.

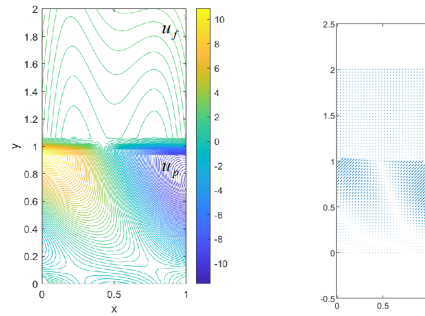


Figure 6: The contour (left) and the vector (right) of the numerical solution for Example 1 Case 2.

Table 4

The comparison between the GFDM and the FEDDM [20] for Example 1 Case 2

	N_x	h	u_f		p		ϕ		u_p		CPU(s)
			$L_{2,relative}$	$H^1_{relative}$	$L_{2,relative}$	$H^1_{relative}$	$L_{2,relative}$	$H^1_{relative}$	$L_{2,relative}$	$H^1_{relative}$	
4th GFDM $m = 40$	8		1.09×10^{-1}	1.29×10^{-1}	3.56×10^{-1}	2.03×10^{-0}	2.76×10^{-2}	5.34×10^{-2}	2.76×10^{-2}	5.34×10^{-2}	0.15
	16		4.45×10^{-3}	4.94×10^{-3}	1.39×10^{-2}	7.88×10^{-2}	1.20×10^{-3}	5.17×10^{-3}	1.20×10^{-3}	5.17×10^{-3}	0.19
	32		2.26×10^{-4}	2.35×10^{-4}	6.97×10^{-4}	3.92×10^{-3}	5.26×10^{-5}	3.82×10^{-4}	5.26×10^{-5}	3.82×10^{-4}	0.41
	64		1.27×10^{-5}	1.26×10^{-5}	3.90×10^{-5}	2.18×10^{-4}	2.80×10^{-6}	2.97×10^{-5}	2.80×10^{-6}	2.97×10^{-5}	1.44
FEDDM[20]		$\frac{1}{8}$	3.25×10^{-2}	7.33×10^{-1}	2.02×10^{-1}	1.42×10^{-1}	1.34×10^{-1}	2.80×10^{-0}	1.34×10^{-1}	2.80×10^{-0}	
		$\frac{1}{16}$	8.14×10^{-3}	3.65×10^{-1}	6.64×10^{-2}	7.04×10^{-2}	3.44×10^{-2}	1.41×10^{-0}	3.44×10^{-2}	1.41×10^{-0}	
		$\frac{1}{32}$	2.04×10^{-3}	1.82×10^{-1}	2.27×10^{-2}	3.51×10^{-2}	8.68×10^{-3}	7.04×10^{-1}	8.68×10^{-3}	7.04×10^{-1}	
		$\frac{1}{64}$	5.10×10^{-4}	9.11×10^{-2}	7.90×10^{-3}	1.75×10^{-2}	2.18×10^{-3}	3.52×10^{-1}	2.18×10^{-3}	3.52×10^{-1}	

$$\mathbf{u}_p = -K \nabla \phi.$$

The biggest feature of these exact solutions is that the p and ϕ are all related to the kinematic viscosity ν of the fluid and the element of the hydraulic conductivity tensor K . In order to examine the proposed meshless GFDM is also applicable with the realistic physical parameters is of practical interest, which is proposed by Ref[20]. We consider the Stokes-Darcy coupled problem with a varying kinematic viscosity ν of the fluid and the element of the hydraulic conductivity tensor K . In this example, the computational subdomains are $\Omega_f = [0, 1] \times [1, 2]$, $\Omega_p = [0, 1] \times [0, 1]$ and $\Gamma = (0, 1) \times [1]$ and we adopt the initial coefficients $\nu = 1$, $K = 1$, $g = 1$ and $\alpha = 1$.

The contour (left) and the vector (right) of the numerical solution are shown in Fig. 7. From Fig. 8 and Fig. 9, we can see that all results are accurate, stable and maintain 2nd order convergence. In particular, the H^1 and $H^1_{relative}$

Table 5

The $L_{2,relative}$ errors when the different order GFDMs are adopted for Example 1 Case 2

	N_x	u_f		p		ϕ		u_p		$CPU(s)$
		$L_{2,relative}$	Order	$L_{2,relative}$	Order	$L_{2,relative}$	Order	$L_{2,relative}$	Order	
4th-order GFDM $m = 40$	16	4.45×10^{-3}	—	1.39×10^{-2}	—	7.88×10^{-2}	—	1.20×10^{-3}	—	0.18
	32	2.26×10^{-4}	4.30	6.97×10^{-4}	4.32	3.92×10^{-3}	4.33	5.26×10^{-5}	4.51	0.40
	64	1.27×10^{-5}	4.15	3.90×10^{-5}	4.16	2.18×10^{-4}	4.17	2.80×10^{-6}	4.23	1.56
	128	7.55×10^{-7}	4.08	2.31×10^{-6}	4.08	1.28×10^{-5}	4.09	1.68×10^{-7}	4.06	14.9
6th-order GFDM $m = 140$	16	2.55×10^{-4}	—	8.02×10^{-4}	—	5.33×10^{-3}	—	2.08×10^{-4}	—	0.61
	32	2.15×10^{-6}	6.89	6.76×10^{-6}	6.89	4.33×10^{-5}	6.95	1.86×10^{-6}	6.81	4.26
	64	2.44×10^{-8}	6.47	7.61×10^{-8}	6.47	4.16×10^{-7}	6.70	2.61×10^{-8}	6.15	23.0
	128	1.94×10^{-10}	6.97	7.63×10^{-10}	6.64	3.47×10^{-9}	6.91	5.17×10^{-10}	5.66	102.0

Table 6

The $H^1_{relative}$ errors when the different order GFDMs are adopted for Example 1 Case 2

	N_x	u_f		p		ϕ		u_p		$CPU(s)$
		$H^1_{relative}$	Order	$H^1_{relative}$	Order	$H^1_{relative}$	Order	$H^1_{relative}$	Order	
4th-order GFDM $m = 50$	16	4.91×10^{-3}	—	9.60×10^{-3}	—	1.41×10^{-3}	—	6.67×10^{-3}	—	0.21
	32	2.25×10^{-4}	4.45	5.69×10^{-4}	4.08	6.31×10^{-5}	4.49	4.57×10^{-4}	3.87	0.44
	64	1.19×10^{-5}	4.24	3.78×10^{-5}	3.91	3.12×10^{-6}	4.33	3.07×10^{-5}	3.90	1.84
	128	6.84×10^{-7}	4.13	2.65×10^{-6}	3.84	1.73×10^{-7}	4.18	2.21×10^{-6}	3.80	11.1
6th-order GFDM $m = 140$	16	2.88×10^{-4}	—	6.19×10^{-4}	—	2.07×10^{-4}	—	8.55×10^{-4}	—	0.75
	32	2.69×10^{-6}	6.75	7.88×10^{-6}	6.30	1.97×10^{-6}	6.71	2.27×10^{-5}	5.23	2.79
	64	3.31×10^{-8}	6.34	1.21×10^{-7}	6.03	2.60×10^{-8}	6.25	3.78×10^{-7}	5.91	12.1
	128	3.29×10^{-10}	6.65	2.46×10^{-9}	5.62	5.13×10^{-10}	5.66	5.76×10^{-9}	6.04	82.0

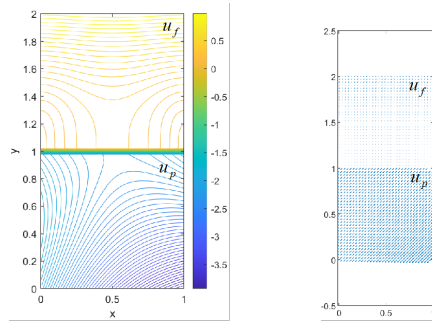

Figure 7: The contour(left) and the vector (right) of numerical solution for Example 2.

Table 7

The L_2 and H^1 relative errors and CPU (s) of the GFDM for Example 2

	N_x	u_f		p		ϕ		u_p	$CPU(s)$
		$L_{2,relative}$	$H^1_{relative}$	$L_{2,relative}$	$L_{2,relative}$	$L_{2,relative}$			
2nd GFDM	8	3.79×10^{-2}	3.98×10^{-2}	6.03×10^{-3}	4.97×10^{-2}	8.81×10^{-3}		0.15	
	16	4.20×10^{-3}	4.83×10^{-3}	6.59×10^{-4}	4.79×10^{-3}	1.88×10^{-3}		0.10	
	32	4.85×10^{-4}	5.81×10^{-4}	7.61×10^{-5}	4.24×10^{-4}	4.42×10^{-4}		0.17	
	64	5.79×10^{-5}	7.06×10^{-5}	9.11×10^{-6}	5.69×10^{-5}	1.08×10^{-4}		1.14	
	128	7.05×10^{-6}	8.67×10^{-6}	1.11×10^{-6}	1.85×10^{-5}	2.69×10^{-5}		6.18	

errors for the Darcy velocity \mathbf{u}_p are also accurate and can keep 1.5 order convergence. It means our method can also perform well in the second order derivatives and have no error accumulation, which is in good agreement with the above conclusion that it can show the advantage of the GFDM for the derivative functions. In Table 7, the L_2 and H^1 relative errors of the GFDM are presented. From this table, we can see that our method is accurate and high efficiency due to the CPU time is very small. The varying kinematic viscosity of fluid ν can be set $\nu = 1.0, 10^{-2}, 10^{-4}, 10^{-6}, 10^{-8}$. The L_2 errors for the numerical velocity of Stokes \mathbf{u}_f (left) and Darcy \mathbf{u}_p (right) with varying ν are shown in Fig. 10. From these figures, we can see the numerical results support that the meshless GFDM are accurate and keep 2nd order convergence. Furthermore, some numerical results with the different realistic parameters $\nu = 0.1, 0.01, 0.001$ and $K = 1.0, 0.1$ are shown in Fig. 11. We can see that the numerical results are also accurate and keep 2nd order convergence. It means

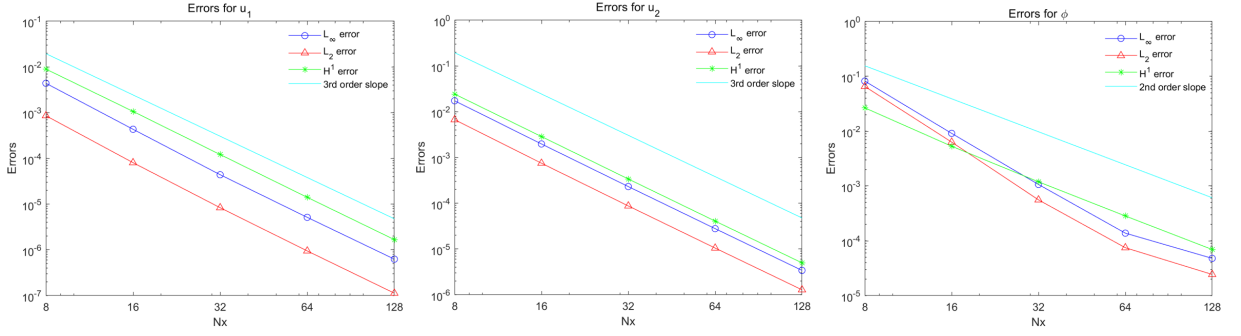


Figure 8: L_∞, L_2 and H^1 errors of the component functions for Example 2.

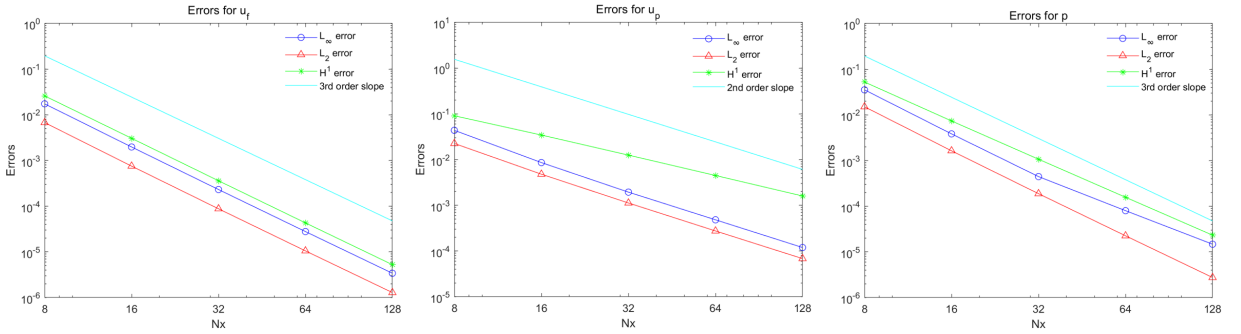


Figure 9: L_∞, L_2 and H^1 errors of fluid velocity u_f (left), Darcy velocity u_p (middle) and pressure p (right) for Example 2.

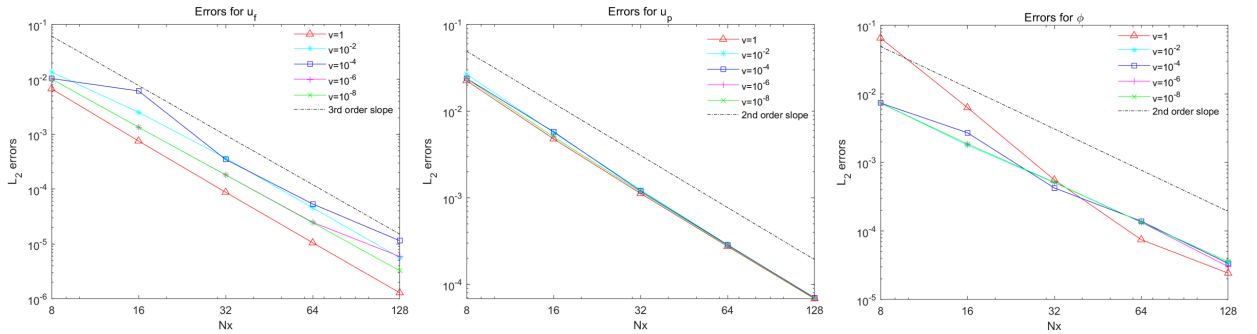


Figure 10: The L_2 errors for the numerical velocity of Stokes u_f (left), Darcy u_p (middle) and ϕ (right) with varying the kinematic viscosity of fluid ν for Example 2.

that our meshless method can do well in the Stokes-Darcy coupled problem in realistic applications. In this example we also test the stability about the 'm'. Note that our numerical errors are all kept at the same accuracy and our results are all stable in the range from 12 to 22. In this example, we adopt $m = 20$.

5.3. Example 3: The Stokes-Darcy coupled problem with closed complex interfaces.

In this example, we consider the first problem with a circle interface (see Fig.12) $\Gamma : \varphi = x^2 + y^2 - 0.25 = 0$. This problem is inspired by Li[24], which considers the Stokes-Darcy coupled problem with closed interface and makes a channel flow outside the circle and the porous media flow inside the interface. Furthermore, in order to show the advantage of the GFDM for complex interface, we consider the following complex interfaces:

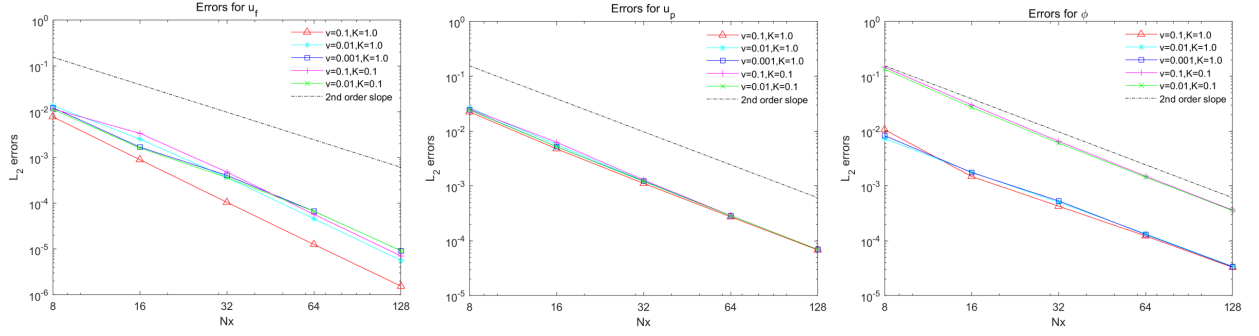


Figure 11: The L_2 errors for the numerical velocity of Stokes \mathbf{u}_f (left), Darcy \mathbf{u}_p (middle) and ϕ (right) with different parameters for Example 2.

Table 8

L_∞, L_2 and H^1 errors of the GFDM with different m when $N_x = 32$ for Example 2

m	\mathbf{u}_f			\mathbf{u}_p			\mathbf{p}			ϕ	
	L_∞	L_2	H^1	L_∞	L_2	$H^{1,relative}$	L_2	H^1	L_2	H^1	
12	1.60×10^{-4}	6.06×10^{-5}	2.49×10^{-4}	1.58×10^{-3}	1.26×10^{-3}	1.68×10^{-2}	1.31×10^{-4}	7.44×10^{-4}	3.54×10^{-4}	1.31×10^{-3}	
14	1.88×10^{-4}	7.10×10^{-5}	2.91×10^{-4}	1.80×10^{-3}	1.24×10^{-3}	1.49×10^{-2}	1.53×10^{-4}	8.75×10^{-4}	4.11×10^{-4}	1.30×10^{-3}	
16	2.25×10^{-4}	8.53×10^{-5}	3.50×10^{-4}	2.07×10^{-3}	1.26×10^{-3}	1.41×10^{-2}	1.84×10^{-4}	1.04×10^{-3}	5.13×10^{-4}	1.32×10^{-3}	
18	2.25×10^{-4}	8.53×10^{-5}	3.50×10^{-4}	1.93×10^{-3}	1.24×10^{-3}	1.38×10^{-2}	1.84×10^{-4}	1.04×10^{-3}	5.14×10^{-4}	1.31×10^{-3}	
20	2.31×10^{-4}	8.78×10^{-5}	3.60×10^{-4}	1.94×10^{-3}	1.12×10^{-3}	1.25×10^{-2}	1.89×10^{-4}	1.07×10^{-3}	5.58×10^{-4}	1.19×10^{-3}	
22	2.39×10^{-4}	9.05×10^{-5}	3.72×10^{-4}	1.99×10^{-3}	9.44×10^{-4}	1.18×10^{-2}	1.95×10^{-4}	1.10×10^{-3}	6.10×10^{-4}	1.01×10^{-3}	

Table 9

The L_2 and H^1 relative errors and CPU(s) of the GFDM for Example 3

	N_x	\mathbf{u}_f		p		ϕ		\mathbf{u}_p		CPU(s)
		$L_{2,relative}$	$H^1_{relative}$	$L_{2,relative}$	$L_{2,relative}$	$L_{2,relative}$	$H^1_{relative}$	$L_{2,relative}$	$H^1_{relative}$	
2nd GFDM	16	2.74×10^{-2}	5.93×10^{-2}	3.24×10^{-2}	1.88×10^{-1}	3.40×10^{-2}	2.41×10^{-1}	3.40×10^{-2}	2.41×10^{-1}	0.22
	32	8.25×10^{-3}	1.48×10^{-2}	8.30×10^{-3}	8.32×10^{-2}	6.69×10^{-3}	8.13×10^{-2}	6.69×10^{-3}	8.13×10^{-2}	0.23
	64	1.63×10^{-3}	2.85×10^{-3}	1.66×10^{-3}	1.82×10^{-2}	1.82×10^{-3}	3.11×10^{-2}	1.82×10^{-3}	3.11×10^{-2}	0.52
	128	4.36×10^{-4}	6.93×10^{-4}	4.26×10^{-4}	5.14×10^{-3}	3.62×10^{-4}	1.00×10^{-2}	3.62×10^{-4}	1.00×10^{-2}	2.10

(1) Two-petaled interface:

$$r(\theta) = \begin{cases} x(\theta) = 0.5\cos(\theta) + 0.2\sin(2\theta)\cos(\theta), \\ y(\theta) = 0.5\sin(\theta) + 0.2\sin(2\theta)\sin(\theta), \end{cases} \quad 0 \leq \theta \leq 2\pi. \quad (128)$$

(2) Flower shaped interface:

$$r(\theta) = \begin{cases} x(\theta) = 0.5\cos(\theta) + 0.2\sin(5\theta)\cos(\theta), \\ y(\theta) = 0.5\sin(\theta) + 0.2\sin(5\theta)\sin(\theta), \end{cases} \quad 0 \leq \theta \leq 2\pi. \quad (129)$$

(3) Heart shaped interface:

$$r(\theta) = \begin{cases} x(\theta) = 0.3(1 - \sin(\theta))\cos(\theta), \\ y(\theta) = 0.3(1 - \sin(\theta))\sin(\theta) + 0.2, \end{cases} \quad 0 \leq \theta \leq 2\pi. \quad (130)$$

Fig.12 presents the point collocation, we can see the point distribution of the circle interface. From Fig. 13, we can see the distribution of the numerical solution. In Fig.14 and Fig. 15, we can see the closed circle interface doesn't have any influence on the numerical results of the Stokes-Darcy coupled problem. In particular, the $H^1_{relative}$ errors for the Darcy velocity \mathbf{u}_p are also accurate and can keep 2nd order convergence. It means that the meshless GFDM is efficient for this circle interface problem. Table 9 presents the L_2 and H^1 relative errors of the GFDM and the numerical results are accurate and highly efficient because the CPU time is very small. The interface shape may need more 'm', therefore, we also test the stability about the 'm'. Note that our numerical errors are all kept at almost the same accuracy and our results are all stable in the range from 12 to 22. In this example, we adopt $m = 20$.

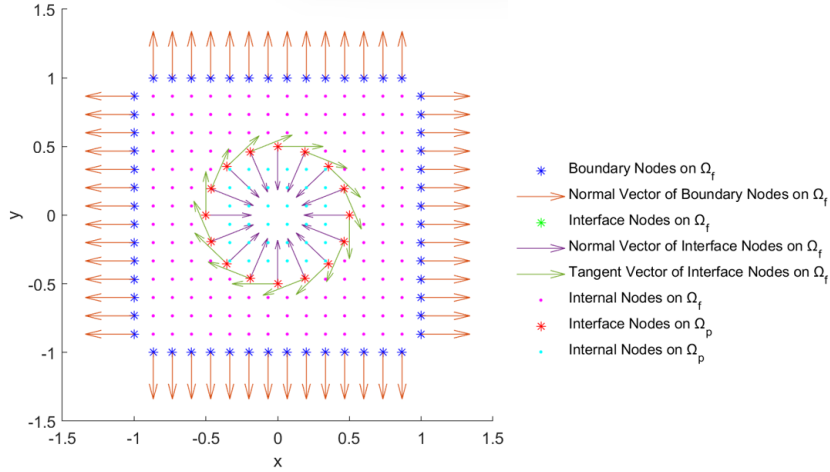


Figure 12: The point collocation for Example 3.

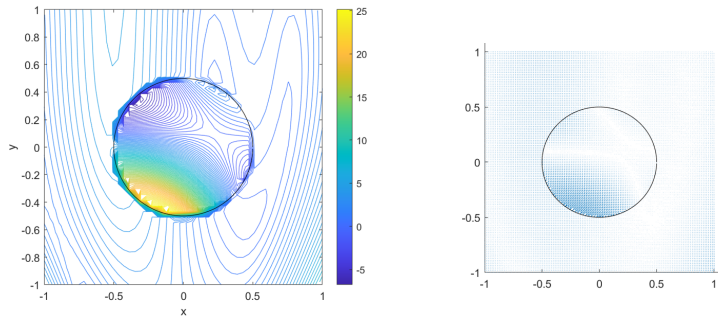


Figure 13: The contour (left) and vector (right) of numerical solution for Example 3.

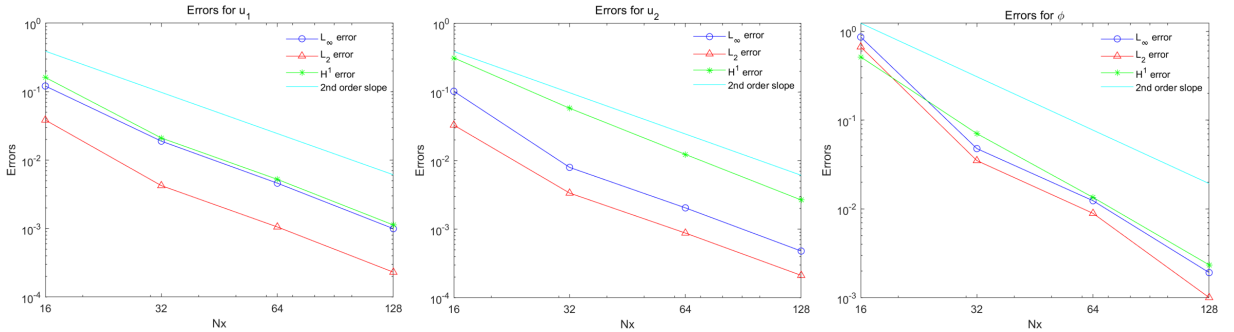


Figure 14: L_∞ , L_2 and H^1 errors of the component functions for Example 3.

In order to test the stability of the complexity of the interface shape, we consider three types of complex interfaces, the point collocation of each one are shown in Fig.16, the explanation of points and vectors is the same as the Fig. 12, we can see that the interface shape and the distributions of the normal vector and the tangent. The contour and vector of the numerical solution are shown in Fig.17 and Fig. 18, we observe that the regular distribution of the numerical solutions. The L_∞ , L_2 and H^1 errors of fluid velocity \mathbf{u}_f (left), Darcy velocity \mathbf{u}_p (middle) and pressure p (right) under these three types of interfaces are shown in Fig.19-Fig.21. Note that the numerical errors are all efficient and keep 2nd order convergence, but the H^1 error of the \mathbf{u}_p has a little oscillation, we don't show the lines. Therefore, there is little impact on the numerical results of the GFDM for the Stokes-Darcy coupled problem with the complex

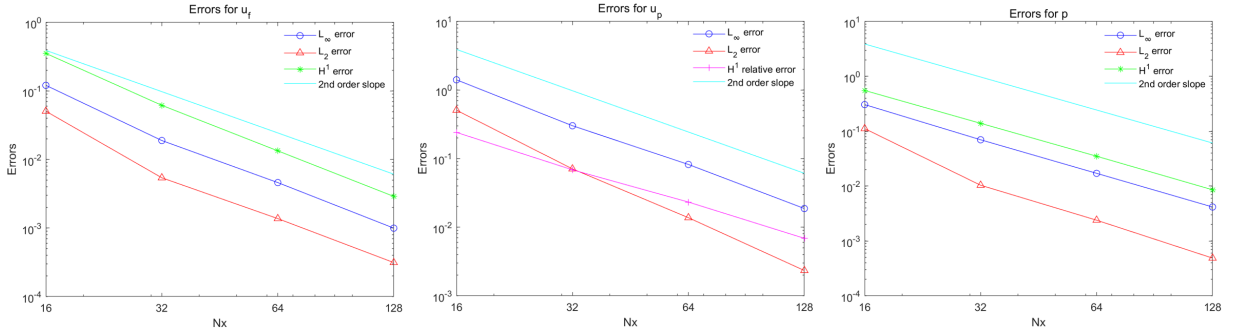


Figure 15: L_∞ , L_2 and H^1 errors of fluid velocity \mathbf{u}_f (left), Darcy velocity \mathbf{u}_p (middle) and pressure p (right) for Example 3.

Table 10

L_∞ , L_2 and H^1 errors of the GFDM with different m when $N_x = 32$ for Example 3

m	\mathbf{u}_f			\mathbf{u}_p			p		ϕ	
	L_∞	L_2	H^1	L_∞	L_2	$H^{1,relative}$	L_2	H^1	L_2	H^1
12	3.36×10^{-2}	7.13×10^{-3}	6.73×10^{-2}	6.89×10^{-1}	1.21×10^{-1}	9.26×10^{-2}	1.42×10^{-2}	1.12×10^{-1}	8.11×10^{-2}	1.20×10^{-1}
14	2.73×10^{-2}	1.15×10^{-2}	7.43×10^{-2}	4.62×10^{-1}	1.02×10^{-1}	7.84×10^{-2}	2.48×10^{-2}	1.15×10^{-1}	1.65×10^{-1}	1.01×10^{-1}
16	2.17×10^{-2}	9.24×10^{-3}	6.89×10^{-2}	3.66×10^{-1}	8.74×10^{-2}	7.27×10^{-2}	1.92×10^{-2}	1.09×10^{-1}	1.23×10^{-1}	8.68×10^{-2}
18	1.97×10^{-2}	5.77×10^{-3}	6.31×10^{-2}	3.06×10^{-1}	7.16×10^{-2}	6.57×10^{-2}	1.06×10^{-2}	1.26×10^{-1}	4.49×10^{-2}	7.18×10^{-2}
20	1.89×10^{-2}	5.41×10^{-3}	6.17×10^{-2}	3.01×10^{-1}	7.08×10^{-2}	6.86×10^{-2}	1.04×10^{-2}	1.40×10^{-1}	3.50×10^{-2}	7.06×10^{-2}
22	1.89×10^{-2}	5.88×10^{-3}	6.28×10^{-2}	3.13×10^{-1}	7.44×10^{-2}	7.34×10^{-2}	1.06×10^{-2}	1.37×10^{-1}	2.99×10^{-2}	7.39×10^{-2}

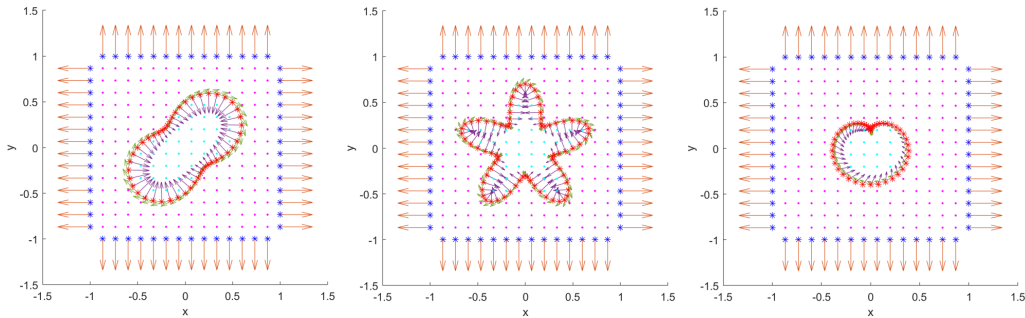


Figure 16: The point collocations under different complex interfaces for Example 3.

interfaces. The interface complexity may need more 'm', Therefore, we test the stability about the 'm' in the range 22 to 40 in Table. 11. Note that our numerical errors are kept at almost the same accuracy and our results are all stable, even in the number of points is small. In this subsection, we adopt $m = 36$.

5.4. Example 4: The Stokes-Darcy coupled problem with the moving interface.

In this example, we also consider the first problem with two moving circle interfaces (see Fig.22) from Ref.[36], in which we can see the specific expression and consider $n = 5$. This problem is also inspired by Li[24], which makes a channel flow outside the circle and the porous media flow inside the interface, and Xing and Zheng [36], which considers the anisotropic elliptic problem with moving interface. In this example, we test the influence of the interface location for the Stokes-Darcy coupled problem.

Fig. 23 and Fig. 28 present the point collocations and moving directions of the proposed problems with the petagon interface and the ellipse interface. we can see the moving directions and the interface location at the specific time. The numerical solutions at each time are shown in Fig.24 and Fig.29. We can see the distributions of the numerical solutions. Figs.25-27 present the numerical results of the GFDM for the Stokes-Darcy coupled problems with petagon interface when $t = 0.1$ (left), $t = 0.5$ (middle) and $t = 1$ (right). Note that the L_∞ , L_2 and H^1 errors are all accurate, stable and keep 2nd order convergence. It means that the interface location has little influence on the numerical results

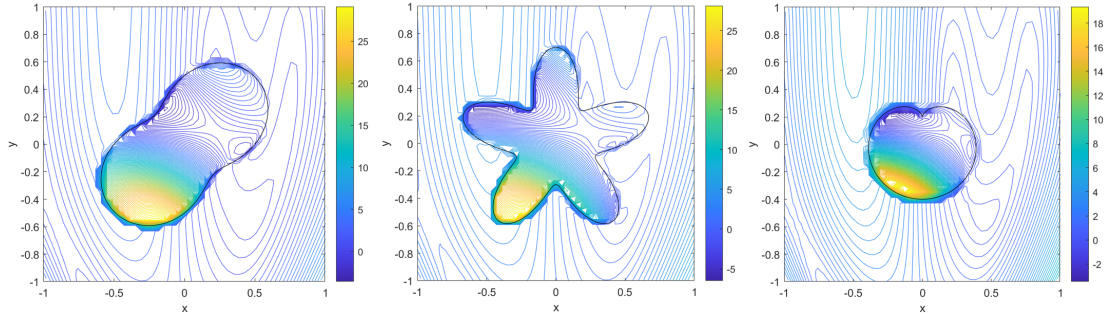


Figure 17: The contour of numerical solutions under different complex interfaces for Example 3.

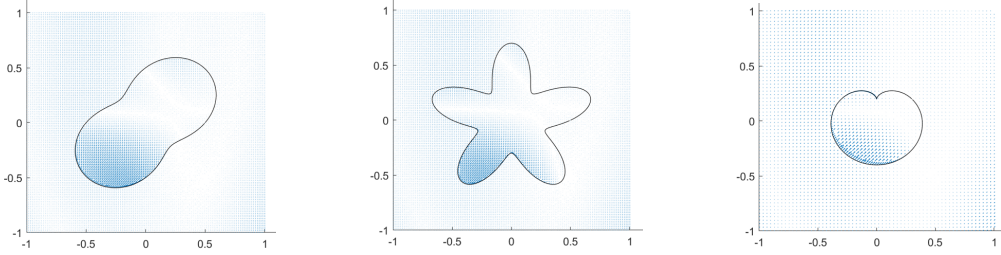


Figure 18: The vector of numerical solutions under different complex interfaces for Example 3.

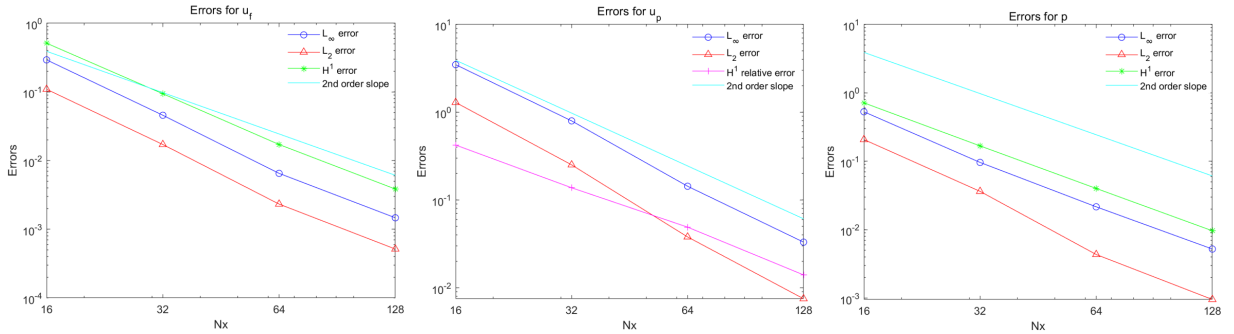


Figure 19: L_∞ , L_2 and H^1 errors of fluid velocity u_f (left), Darcy velocity u_p (middle) and pressure p (right) under the two-petaled interface for Example 3.

of the proposed GFDM for the proposed problem with petagon interface. Figs.30-32 present the numerical results of the GFDM for the Stokes-Darcy coupled problems with ellipse interface when $t = 0.1$ (left), $t = 0.5$ (middle) and $t = 1$ (right). We can see the same conclusion. It means that the interface location has little influence on the numerical results of the proposed GFDM for the proposed problem with ellipse interface. The CPU times of the GFDM when $N_x = 60$, $t = 1$ for Example 3 and Example 4 is presented in Table. 12. From this table we can see the high efficiency of the proposed GFDM for the Stokes-Darcy coupled problem with the proposed all types of closed interfaces. The interface location may need different 'm', therefore, we also test the stability about the 'm' for the proposed problem with petagon interface in Table.13. Note that our numerical errors are all keep at almost the same accuracy and our results are all stable in the range from 22 to 40. The 'm' can be tested for the Stokes-Darcy problem with ellipse interface and we can get almost the same conclusion. In this example, we adopt $m = 36$.

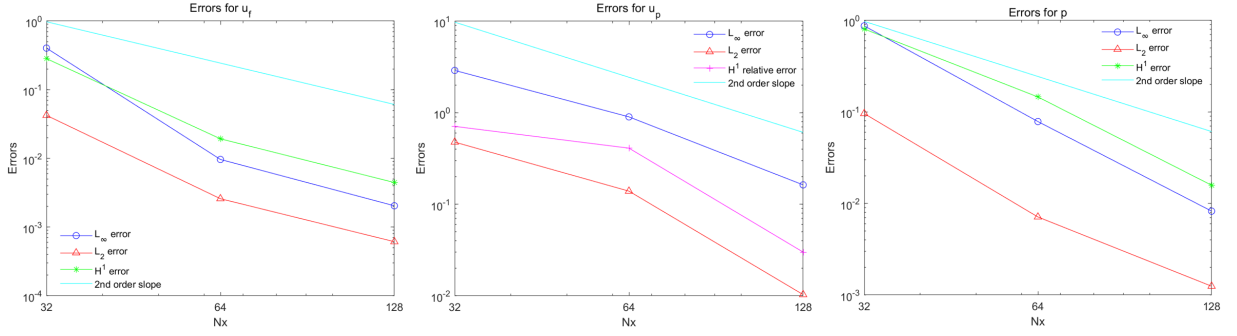


Figure 20: L_∞ , L_2 and H^1 errors of fluid velocity \mathbf{u}_f (left), Darcy velocity \mathbf{u}_p (middle) and pressure p (right) under flower shaped interface for Example 3.

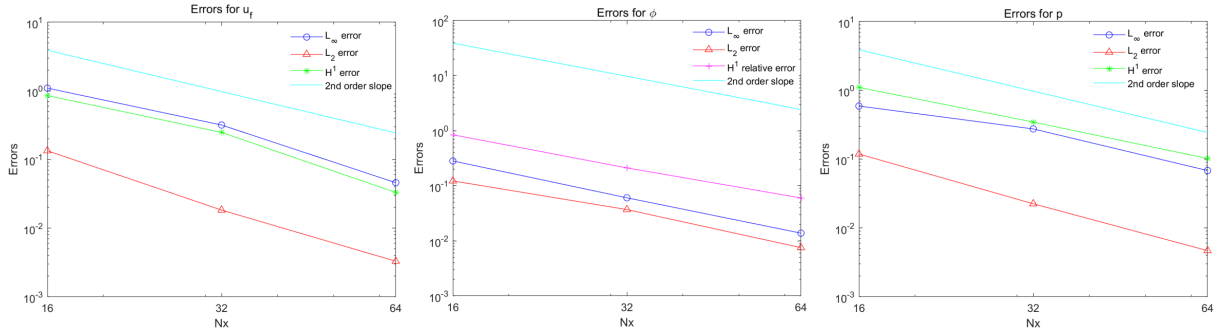


Figure 21: L_∞ , L_2 and H^1 errors of fluid velocity \mathbf{u}_f (left), Darcy velocity \mathbf{u}_p (middle) and pressure p (right) under heart shaped interface for Example 3.

Table 11

L_∞ , L_2 and H^1 errors of the GFDM with different m when $N_x = 32$ for Example 3

	m	u_f		u_p		p	ϕ	
		L_2	H^1	L_2	L_2	H^1	L_2	H^1
Two-petaled interface	22	1.61×10^{-2}	8.11×10^{-2}	2.12×10^{-1}	3.69×10^{-2}	1.65×10^{-1}	9.13×10^{-2}	1.65×10^{-1}
	26	1.75×10^{-2}	8.90×10^{-2}	2.34×10^{-1}	3.85×10^{-2}	1.65×10^{-1}	9.28×10^{-2}	1.79×10^{-1}
	30	1.66×10^{-2}	8.70×10^{-2}	2.29×10^{-1}	3.59×10^{-2}	1.63×10^{-1}	8.61×10^{-2}	1.79×10^{-1}
	32	1.81×10^{-2}	9.10×10^{-2}	2.47×10^{-1}	3.89×10^{-2}	1.64×10^{-1}	9.43×10^{-2}	1.93×10^{-1}
	36	1.71×10^{-2}	9.40×10^{-2}	2.51×10^{-1}	3.63×10^{-2}	1.68×10^{-1}	8.87×10^{-2}	1.96×10^{-1}
	40	2.08×10^{-2}	1.09×10^{-1}	2.85×10^{-1}	4.36×10^{-2}	1.85×10^{-1}	1.06×10^{-1}	2.23×10^{-1}
Flower shaped interface	22	1.42×10^{-2}	8.81×10^{-2}	1.68×10^{-1}	2.84×10^{-2}	2.80×10^{-1}	8.39×10^{-2}	1.68×10^{-1}
	26	1.40×10^{-2}	8.90×10^{-2}	1.99×10^{-1}	2.90×10^{-2}	2.68×10^{-1}	8.57×10^{-2}	1.98×10^{-1}
	30	3.65×10^{-2}	2.52×10^{-1}	1.30×10^{-0}	8.46×10^{-2}	1.49×10^{-0}	2.52×10^{-1}	1.30×10^{-0}
	32	3.97×10^{-2}	2.62×10^{-1}	1.34×10^{-0}	8.47×10^{-2}	1.48×10^{-0}	2.47×10^{-1}	1.33×10^{-0}
	36	4.23×10^{-2}	2.84×10^{-1}	4.77×10^{-1}	9.60×10^{-2}	8.06×10^{-1}	1.21×10^{-1}	5.05×10^{-1}
	40	3.07×10^{-2}	2.10×10^{-1}	5.28×10^{-1}	7.64×10^{-2}	6.52×10^{-1}	1.33×10^{-1}	5.17×10^{-1}

6. Conclusion

In this paper, a meshless generalized finite difference method is proposed to solve the Stokes-Darcy coupled problem with BJS interface conditions. We adopt some high order GFDMs to show the high order accuracy and the convergence order of the GFDMs for Stokes-Darcy coupled problem. Some Stokes-Darcy coupled problems with closed interface which has more complex geometric shape are given to show the accuracy and stability of the GFDM. The interface location has been changed to show that the little influence of the interface location for the Stokes-Darcy coupled problem. Numerical results show that the better accuracy and stability can be obtained by GFDM compared with other high efficient numerical methods.

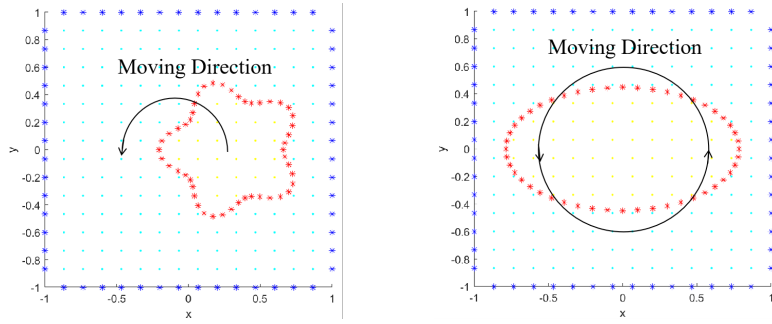


Figure 22: The point collocations and moving directions of the proposed problems with the petagon interface and ellipse interface for Example 4.

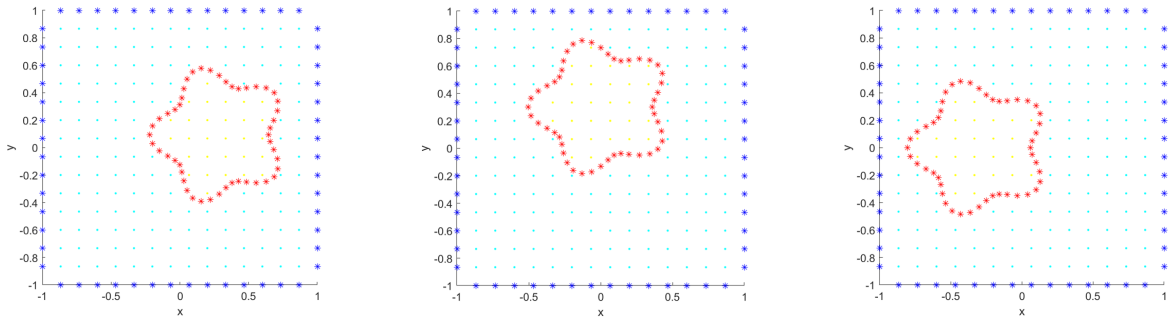


Figure 23: The point collocation when $t = 0.1$ (left), $t = 0.5$ (middle) and $t = 1$ (right) under the petagon interface for Example 4.

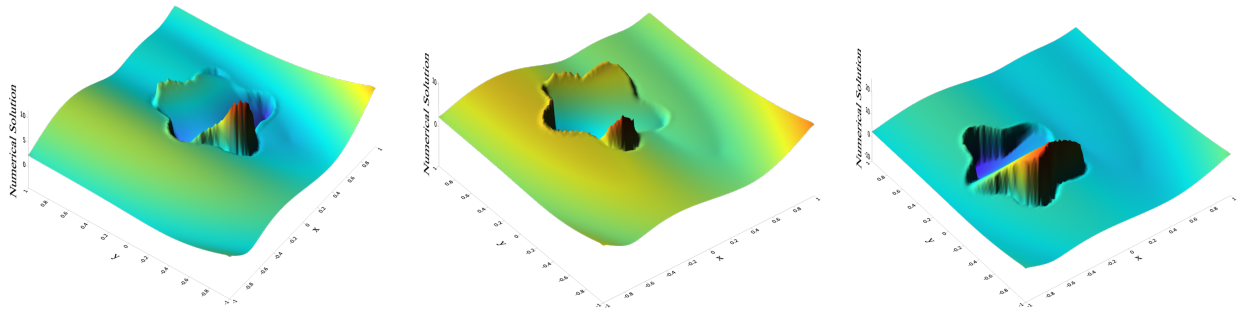


Figure 24: The numerical solution when $t = 0.1$ (left), $t = 0.5$ (middle) and $t = 1$ (right) under the petagon interface for Example 4

Acknowledgments

This work is partially supported by Science and Technology Commission of Shanghai Municipality (Grant Nos. 22JC1400900, 22DZ2229014).

References

- [1] Y. Cao, M. Gunzburger, X. Hu, F. Hua, X. Wang, W. Zhao, Finite element approximations for Stokes-Darcy flow with Beavers-Joseph interface conditions, SIAM J. Numer. Anal., 47, 4239-4256 (2010).

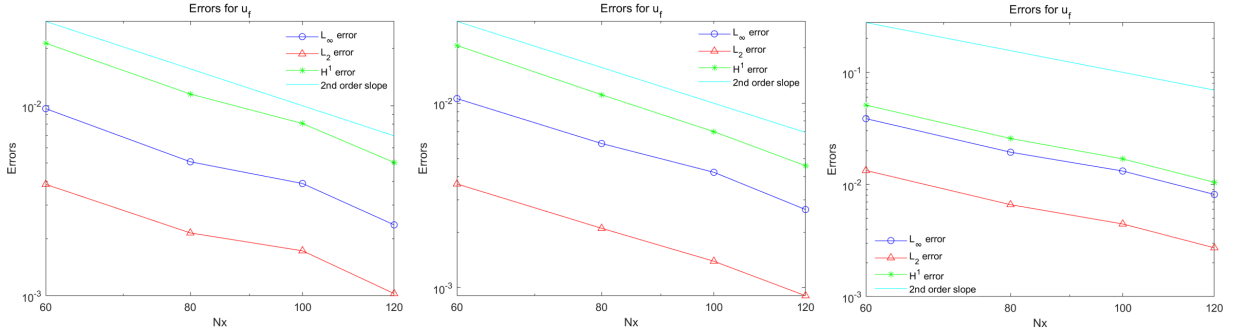


Figure 25: L_∞, L_2 and H^1 errors of u_f when $t = 0.1$ (left), $t = 0.5$ (middle) and $t = 1$ (right) under the petagon interface for Example 4.

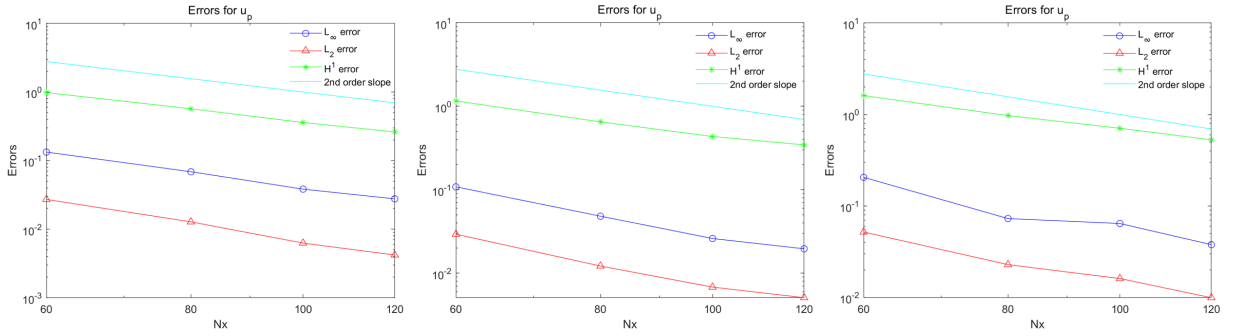


Figure 26: L_∞, L_2 and H^1 errors of u_p when $t = 0.1$ (left), $t = 0.5$ (middle) and $t = 1$ (right) under the petagon interface for Example 4.

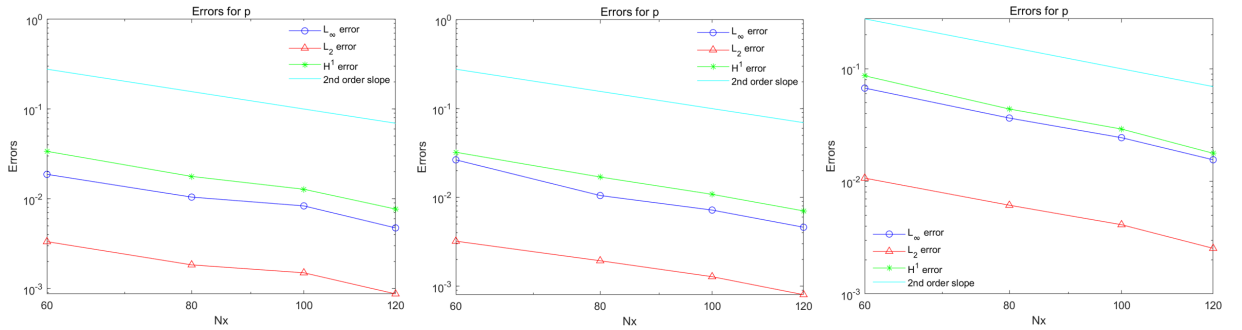


Figure 27: L_∞, L_2 and H^1 errors of p when $t = 0.1$ (left), $t = 0.5$ (middle) and $t = 1$ (right) under the petagon interface for Example 4.

- [2] H. Rui, R. Zhang, A unified stabilized mixed finite element method for coupling Stokes and Darcy flows, Comput. Methods Appl. Mech. Engrg., 198, 33-36(2009).
- [3] J.P. Yu, Y. Z. Sun, F. Shi, H. B. Zheng, Nitsche's type stabilized finite element method for the fully mixed Stokes-Darcy problem with Beavers-Joseph conditions, Appl. Math. Letters., 110, 106588 (2020).
- [4] MA. A. Mahbub, L. Shan, H. B. Zheng, Uncoupling evolutionary groundwater-surface water flows: stabilized mixed methods in both porous media and fluid regions, Numer. Algor., 92(3), 1837-1874 (2023).
- [5] M. Mu, J. Xu, A two-grid method of a mixed Stokes-Darcy model for coupling fluid flow with porous media flow, SIAM J. Numer. Anal., 45, 1801-1813 (2007).
- [6] M. Cai, M. Mu, J. Xu, Numerical solution to a mixed Navier-Stokes/Darcy model by the two-grid approach, SIAM J. Numer. Anal., 47, 3325-3338 (2009).
- [7] L. Y. Zuo, Y. Hou, A decoupling two-grid algorithm for the mixed Stokes-Darcy model with the Beavers-Joseph interface condition, Numer. Methods PDEs., 30, 1066-1082 (2014).

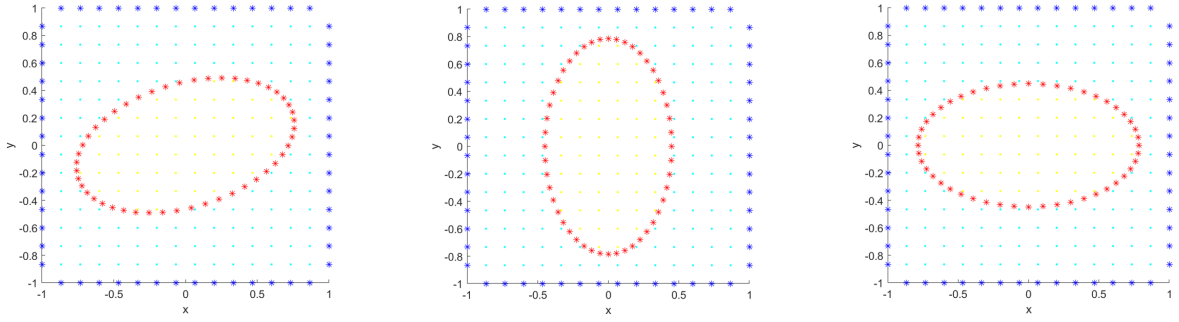


Figure 28: The point collocation when $t = 0.1$ (left), $t = 0.5$ (middle) and $t = 1$ (right) under the ellipse interface for Example 4.

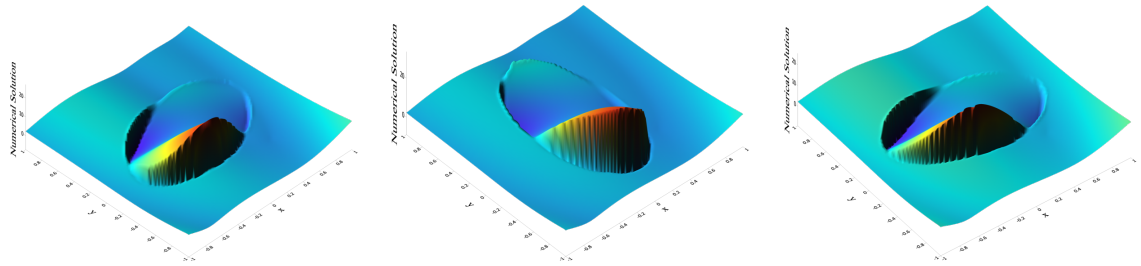


Figure 29: The numerical solution when $t = 0.1$ (left), $t = 0.5$ (middle) and $t = 1$ (right) under the ellipse interface for Example 4.

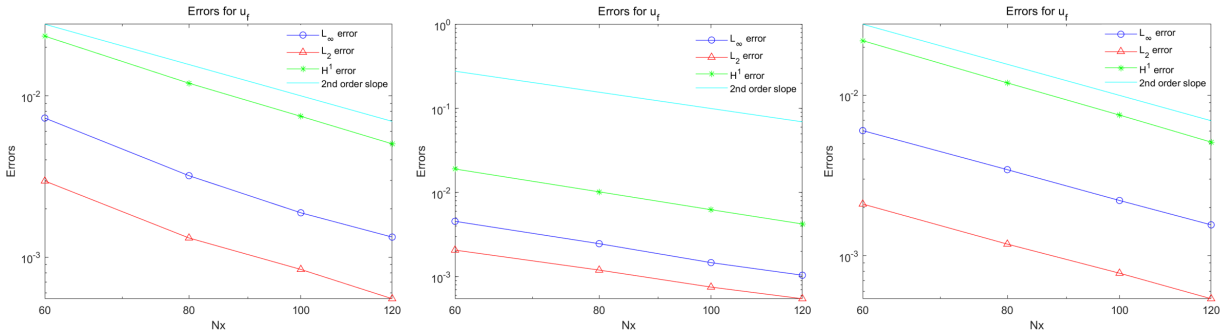


Figure 30: L_∞ , L_2 and H^1 errors of u_f when $t = 0.1$ (left), $t = 0.5$ (middle) and $t = 1$ (right) under the ellipse interface for Example 4.

- [8] Y. Hou, Optimal error estimates of a decoupled scheme based on two-grid finite element for mixed Stokes-Darcy model, App. Math. Letters., 57, 90-96 (2016).
- [9] W. J. Layton, F. Schieweck, I. Yotov, Coupling fluid flow with porous media flow, SIAM J. Numer. Anal., 40, 2195-2218 (2003).
- [10] M. Gunzburger, X. M. He, B. Li, On Stokes-Ritz projection and multistep backward differentiation schemes in decoupling the Stokes-Darcy model, SIAM J. Numer. Anal., 56, 397-427 (2018).
- [11] L. Shan, H. B. Zheng, Partitioned time stepping method for fully evolutionary Stokes-Darcy flow with Beavers-Joseph interface conditions, SIAM J. Numer. Anal., 51, 813-839 (2013).
- [12] L. Shan, H. B. Zheng, W. J. Layton, A decoupling method with different subdomain time steps for the nonstationary Stokes-Darcy model, Numer. Methods PDEs., 29, 549-583 (2013).
- [13] W. Layton, H. Tran, C. Trenchea, Analysis of long time stability and error of two partitioned methods for uncoupling evolutionary groundwater-surface water flows, SIAM J. Numer. Anal., 51, 248-272 (2013).
- [14] M. Discacciati, A. Quarteroni, A. Valli, Robin-Robin domain decomposition methods for the Stokes-Darcy coupling, SIAM J. Numer. Anal.,

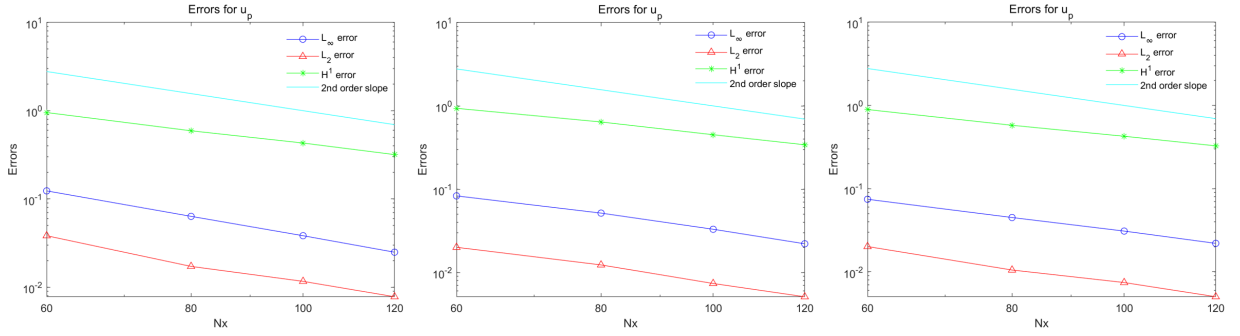


Figure 31: L_∞ , L_2 and H^1 errors of u_p when $t = 0.1$ (left), $t = 0.5$ (middle) and $t = 1$ (right) under the ellipse interface for Example 4.

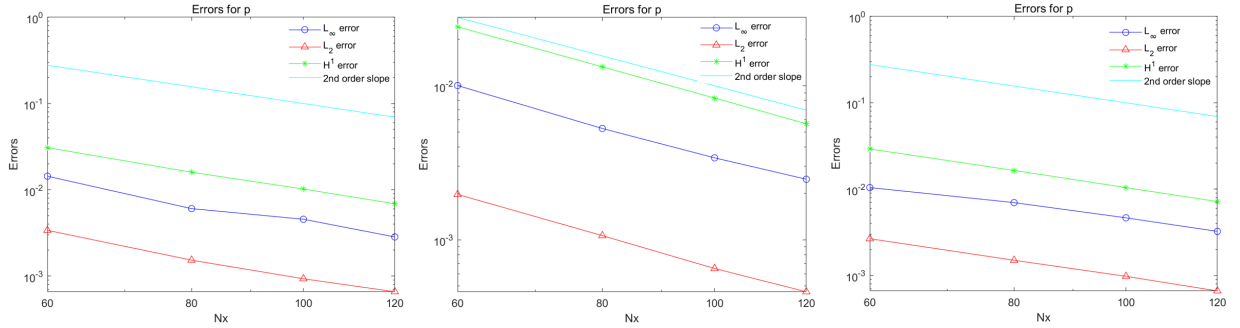


Figure 32: L_∞ , L_2 and H^1 errors of p when $t = 0.1$ (left), $t = 0.5$ (middle) and $t = 1$ (right) under the ellipse interface for Example 4.

Table 12

The CPU times of the GFDM when $N_x = 60, t = 1$ for Example 3 and Example 4

Interface	Example 3				Example 4	
	Circle interface	Two-petaled interface	Flower shaped interface	Heart shaped interface	Petagon interface	Ellipse interface
CPU(s)	0.48	1.39	1.07	1.23	1.25	1.06

Table 13

L_∞ , L_2 and H^1 errors of the GFDM with different m when $N_x = 60, t = 1$ and the petagon interface is used for Example 4

m	u_f			u_p			p		ϕ	
	L_∞	L_2	H^1	L_∞	L_2	$H^{1,relative}$	L_2	H^1	L_2	H^1
22	9.95×10^{-3}	3.46×10^{-3}	2.12×10^{-2}	7.92×10^{-2}	2.64×10^{-2}	3.28×10^{-2}	4.39×10^{-3}	2.78×10^{-2}	2.00×10^{-2}	2.64×10^{-2}
26	1.05×10^{-2}	3.64×10^{-3}	2.25×10^{-2}	8.29×10^{-2}	2.78×10^{-2}	3.46×10^{-2}	4.57×10^{-3}	2.97×10^{-2}	2.07×10^{-2}	2.78×10^{-2}
30	1.12×10^{-2}	3.84×10^{-3}	2.45×10^{-2}	8.75×10^{-2}	3.16×10^{-2}	3.76×10^{-2}	4.93×10^{-3}	3.31×10^{-2}	2.16×10^{-2}	3.15×10^{-2}
36	6.03×10^{-3}	2.10×10^{-3}	2.19×10^{-2}	7.45×10^{-2}	2.02×10^{-2}	3.90×10^{-2}	2.67×10^{-3}	2.92×10^{-2}	9.29×10^{-3}	1.95×10^{-2}
40	6.39×10^{-3}	2.28×10^{-3}	2.53×10^{-2}	8.69×10^{-2}	2.11×10^{-2}	4.08×10^{-2}	2.69×10^{-3}	3.24×10^{-2}	8.96×10^{-3}	2.04×10^{-2}

45, 1246-1268 (2007).

- [15] W. Chen, M. Gunzburger, F. Hua, X. Wang, A parallel Robin-Robin domain decomposition method for the Stokes-Darcy system, SIAM. J. Numer. Anal., 49, 1064-1084 (2011).
- [16] Y. Boubendir, S. Tlupova S, Domain decomposition methods for solving Stokes-Darcy problems with boundary integrals, SIAM J. Sci. Comput., 35, B82-B106 (2013).
- [17] X. M. He, J. Li, Y. P. Lin, J. Ming, A domain decomposition method for the steady-state Navier-Stokes-Darcy model with the Beavers-Joseph interface condition, SIAM J. Sci. Comput., 37, S264-S290 (2015).
- [18] D. Vassilev, C. Wang, I. Yotov, Domain decomposition for coupled Stokes and Darcy flows, Comput. Methods Appl. Mech. Engrg., 268, 264-283 (2014).
- [19] B. Jiang, A parallel domain decomposition method for coupling of surface and groundwater flows, Comput. Methods Appl. Mech. Engrg., 198, 947-957 (2009).
- [20] Y. Z. Sun, W. W. Sun, H. B. Zheng, Domain decomposition method for the fully-mixed Stokes-Darcy coupled problem, Comput. Methods

- Appl. Mech. Engrg., 374, 113578 (2021).
- [21] Y. Z. Sun, F. Shi, H. B. Zheng, H. Li, F. Wang, Two-grid domain decomposition methods for the coupled Stokes-Darcy system, Comput. Methods Appl. Mech. Engrg., 385, 114041 (2021).
 - [22] W. B. Chen, M. Gunzburger, F. Hua, X. M. Wang, Parallel Robin-Robin domain decomposition method for the Stokes-Darcy system, SIAM. J. Numer. Anal., 49(3), 1064-1084 (2011).
 - [23] R. Li, J. Li, Z. X. Chen, Y. L. Gao, A stabilized finite element method based on two local Gauss integrations for a coupled Stokes-Darcy problem, J Comput. Appl. Math., 292, 92-104 (2016).
 - [24] Z. L. Li, An augmented Cartesian grid method for Stokes-Darcy fluid-structure interactions, Int. J. Numer. Meth. Engng., 106, 556-575 (2016).
 - [25] M. Safarpour, A. Shirzadi, Numerical investigation based on radial basis function-finite-difference (RBF-FD) method for solving the Stokes-Darcy equations, Eng. Comput-Germany. 37, 909-920(2021).
 - [26] R. L. Pu, X. L. Feng, Physics-Informed Neural Networks for solving coupled Stokes-Darcy equation, Entropy 24(8), 1106(2022).
 - [27] J. Yue, J. Li, Efficient coupled deep neural networks for the time-dependent coupled Stokes-Darcy problems, Appl. Math. Comput., 437, 127514(2023).
 - [28] J. Orkisz, Meshless finite difference method I Basic approach. Computational mechanics IACM. Idelshon Oñate, Duorkin, editors. CINME; 1998.
 - [29] J. J. Benito, F. Urena and L. Gavete, Influence of several factors in the generalized finite difference method, Appl. Math. Model., 25, 1039-1053 (2011).
 - [30] J. J. Benito, F. Urena and L. Gavete, An h-adaptive method in generalized finite differences, Comput. Methods App. Mech. Eng., 192(5-6), 735-759(2003).
 - [31] L. Gavete, F. Urena, J. J. Benito, A. Garcia, M. Urena, E. Salete, Solving second order non-linear elliptic partial differential equations using generalized finite difference method, J. Comput Appl. Math., 318, 378-387(2017).
 - [32] E. Salete, J. J. Benito, F. Urena, L. Gavete, M. Urena, A. Garcia, Stability of perfectly matched layer regions in generalized finite difference method for wave problems, J. Comput Appl. Math., 312, 231-239(2017).
 - [33] C. M. Fan, P. W. Li, W. C. Yeh, Generalized finite difference method for solving two-dimensional inverse Cauchy problems, Inverse. Probl. Sci. Eng., 23(5), 737-759(2015).
 - [34] Y. Gu, L. Wang, W. Chen, C. Z. Zhang, X. Q. He, Application of the meshless generalized finite difference method to inverse heat source problems, Int. J. Heat. Mass. Transf., 108, 721-729(2017).
 - [35] O. Davydov and M. Safarpour, A meshless finite difference method for elliptic interface problems based on pivoted QR decomposition, Appl. Numer. Math., 161, 489-509 (2021).
 - [36] Y. N. Xing, H. B. Zheng, A high order generalized finite difference method for solving the anisotropic elliptic interface problem in static and moving systems, Comput. Math. Appl., 166C, 1-23(2024).
 - [37] H. Kraus, J. Kuhnert, A. Meister and P. Suchde, A meshfree point collocation method for elliptic interface problems, Appl. Math. Model., 113, 241-261(2023).
 - [38] Y. N. Xing, L. N. Song, X. M. He, C. X. Qiu, A generalized finite difference method for solving elliptic interface problems, Math. Comput. Simulat., 178, 109-124(2020).
 - [39] Y. N. Xing, L. N. Song and C. M. Fan, A generalized finite difference method for solving elasticity interface problems, Eng. Anal. Bound. Elem., 128(1), 105-117(2021).
 - [40] Y. N. Xing, L. N. Song and P. W. Li, A generalized finite difference method for solving biharmonic interface problems, Eng. Anal. Bound. Elem., 135, 132-144 (2022).
 - [41] L. N. Song, P. W. Li, Y. Gu, C. M. Fan, Generalized finite difference method for solving stationary 2D and 3D Stokes equations with a mixed boundary condition, Comput. Math. Appl., 80, 1726-1743(2020).
 - [42] M. R. Shao, L. N. Song and P. W. Li, A generalized finite difference method for solving stokes interface problems, Eng. Anal. Bound. Elem., 132(1), 50-64(2021).
 - [43] D. Shirokoff, I.: A Pressure Poisson Method for the Incompressible Navier-Stokes Equations: II. Long Time Behavior of the Klein-Gordon Equations. PhD thesis, Massachusetts Institute of Technology (2011).
 - [44] J. J. Benito, F. Urena and L. Gavete, Solving parabolic and hyperbolic equations by the generalized finite difference method, J. Comput. Appl. Math., 209, 208-233(2007).

Appendix A

In 2D case, minimizing the residual function of the second-order partial derivatives in the second-order generalized finite difference method, a linear algebraic equation system can be obtained,

$$AD_{2,u} = b_2, \quad (131)$$

let

$$\begin{aligned}
 A &= \begin{pmatrix} \sum_{k=1}^m h_k^2 \omega_k^2 & \sum_{k=1}^m h_k l_k \omega_k^2 & \sum_{k=1}^m \frac{h_k^3}{2} \omega_k^2 & \sum_{k=1}^m \frac{l_k^2 h_k}{2} \omega_k^2 & \sum_{k=1}^m h_k^2 l_k \omega_k^2 \\ \sum_{k=1}^m h_k l_k \omega_k^2 & \sum_{k=1}^m l_k^2 \omega_k^2 & \sum_{k=1}^m \frac{h_k^2 l_k}{2} \omega_k^2 & \sum_{k=1}^m \frac{l_k^3}{2} \omega_k^2 & \sum_{k=1}^m \frac{l_k^2 h_k}{2} \omega_k^2 \\ \sum_{k=1}^m \frac{h_k^3}{2} \omega_k^2 & \sum_{k=1}^m \frac{h_k^2 l_k}{2} \omega_k^2 & \sum_{k=1}^m \frac{h_k^4}{4} \omega_k^2 & \sum_{k=1}^m \frac{l_k^2 h_k^2}{4} \omega_k^2 & \sum_{k=1}^m \frac{h_k^3 l_k}{2} \omega_k^2 \\ \sum_{k=1}^m \frac{l_k^2 h_k}{2} \omega_k^2 & \sum_{k=1}^m \frac{l_k^3}{2} \omega_k^2 & \sum_{k=1}^m \frac{l_k^2 h_k^2}{4} \omega_k^2 & \sum_{k=1}^m \frac{l_k^4}{4} \omega_k^2 & \sum_{k=1}^m \frac{l_k^3 h_k}{2} \omega_k^2 \\ \sum_{k=1}^m h_k^2 l_k \omega_k^2 & \sum_{k=1}^m \frac{l_k^2 h_k}{2} \omega_k^2 & \sum_{k=1}^m \frac{h_k^3 l_k}{2} \omega_k^2 & \sum_{k=1}^m \frac{l_k^3 h_k}{2} \omega_k^2 & \sum_{k=1}^m l_k^2 h_k^2 \omega_k^2 \end{pmatrix} \\
 &= \begin{pmatrix} a_{11} & a_{12} & a_{13} & a_{14} & a_{15} \\ a_{21} & a_{22} & a_{23} & a_{24} & a_{25} \\ a_{31} & a_{32} & a_{33} & a_{34} & a_{35} \\ a_{41} & a_{42} & a_{43} & a_{44} & a_{45} \\ a_{51} & a_{52} & a_{53} & a_{54} & a_{55} \end{pmatrix}
 \end{aligned} \tag{132}$$

then

$$A \begin{pmatrix} \frac{\partial u_0}{\partial x} \\ \frac{\partial^2 u_0}{\partial x^2} \\ \frac{\partial y}{\partial x^2} \\ \frac{\partial^2 u_0}{\partial y^2} \\ \frac{\partial^2 u_0}{\partial x \partial y} \end{pmatrix} = \begin{pmatrix} b_1 \\ b_2 \\ b_3 \\ b_4 \\ b_5 \end{pmatrix} = \begin{pmatrix} \sum_{k=1}^m (-u_0 + u_k) h_k \omega_k^2 \\ \sum_{k=1}^m (-u_0 + u_k) l_k \omega_k^2 \\ \sum_{k=1}^m (-u_0 + u_k) \frac{h_k^2}{2} \omega_k^2 \\ \sum_{k=1}^m (-u_0 + u_k) \frac{l_k^2}{2} \omega_k^2 \\ \sum_{k=1}^m (-u_0 + u_k) h_k l_k \omega_k^2 \end{pmatrix}, \tag{133}$$

Due to the matrix A is symmetrical, it is possible to use the Cholesky method to solve the systems. The upper and lower triangular matrices[44]:

$$A = \begin{pmatrix} a_{11} & a_{12} & a_{13} & a_{14} & a_{15} \\ a_{21} & a_{22} & a_{23} & a_{24} & a_{25} \\ a_{31} & a_{32} & a_{33} & a_{34} & a_{35} \\ a_{41} & a_{42} & a_{43} & a_{44} & a_{45} \\ a_{51} & a_{52} & a_{53} & a_{54} & a_{55} \end{pmatrix} = LL^T = \begin{pmatrix} l_{11} & 0 & 0 & 0 & 0 \\ l_{21} & l_{22} & 0 & 0 & 0 \\ l_{31} & l_{32} & l_{33} & 0 & 0 \\ l_{41} & l_{42} & l_{43} & l_{44} & 0 \\ l_{51} & l_{52} & l_{53} & l_{54} & l_{55} \end{pmatrix} \begin{pmatrix} l_{11} & l_{21} & l_{31} & l_{41} & l_{51} \\ 0 & l_{22} & l_{32} & l_{42} & l_{52} \\ 0 & 0 & l_{33} & l_{43} & l_{53} \\ 0 & 0 & 0 & l_{44} & l_{45} \\ 0 & 0 & 0 & 0 & l_{55} \end{pmatrix}. \tag{134}$$

here

$$l_{i1} = \frac{a_{1i}}{\sqrt{a_{11}}}, i = 1, 2, 3, 4, 5, \tag{135}$$

$$l_{i2} = \frac{a_{2i} - l_{21}l_{i1}}{\sqrt{l_{22}}}, i = 2, 3, 4, 5, \tag{136}$$

$$l_{i3} = \frac{a_{3i} - l_{31}l_{i1} - l_{32}l_{i2}}{\sqrt{l_{33}}}, i = 3, 4, 5, \tag{137}$$

$$l_{i4} = \frac{a_{4i} - l_{41}l_{i1} - l_{42}l_{i2} - l_{43}l_{i3}}{\sqrt{l_{44}}}, i = 4, 5, \tag{138}$$

$$l_{55} = \sqrt{a_{55} - (l_{51}^2 + l_{52}^2 + l_{53}^2 + l_{54}^2)} \tag{139}$$

$$\begin{pmatrix} l_{11} & 0 & 0 & 0 & 0 \\ l_{21} & l_{22} & 0 & 0 & 0 \\ l_{31} & l_{32} & l_{33} & 0 & 0 \\ l_{41} & l_{42} & l_{43} & l_{44} & 0 \\ l_{51} & l_{52} & l_{53} & l_{54} & l_{55} \end{pmatrix} \begin{pmatrix} l_{11} & l_{21} & l_{31} & l_{41} & l_{51} \\ 0 & l_{22} & l_{32} & l_{42} & l_{52} \\ 0 & 0 & l_{33} & l_{43} & l_{53} \\ 0 & 0 & 0 & l_{44} & l_{45} \\ 0 & 0 & 0 & 0 & l_{55} \end{pmatrix} \begin{pmatrix} \frac{\partial u_0}{\partial x} \\ \frac{\partial u_0}{\partial y} \\ \frac{\partial^2 u_0}{\partial x^2} \\ \frac{\partial^2 u_0}{\partial y^2} \\ \frac{\partial^2 u_0}{\partial x \partial y} \end{pmatrix} = \begin{pmatrix} \sum_{k=1}^m (-u_0 + u_k) h_k \omega_k^2 \\ \sum_{k=1}^m (-u_0 + u_k) l_k \omega_k^2 \\ \sum_{k=1}^m (-u_0 + u_k) \frac{h_k^2}{2} \omega_k^2 \\ \sum_{k=1}^m (-u_0 + u_k) \frac{l_k^2}{2} \omega_k^2 \\ \sum_{k=1}^m (-u_0 + u_k) h_k l_k \omega_k^2 \end{pmatrix} \quad (140)$$

$$\begin{pmatrix} \frac{\partial u_0}{\partial x} \\ \frac{\partial u_0}{\partial y} \\ \frac{\partial^2 u_0}{\partial x^2} \\ \frac{\partial^2 u_0}{\partial y^2} \\ \frac{\partial^2 u_0}{\partial x \partial y} \end{pmatrix} = \begin{pmatrix} l_{11} & 0 & 0 & 0 & 0 \\ l_{21} & l_{22} & 0 & 0 & 0 \\ l_{31} & l_{32} & l_{33} & 0 & 0 \\ l_{41} & l_{42} & l_{43} & l_{44} & 0 \\ l_{51} & l_{52} & l_{53} & l_{54} & l_{55} \end{pmatrix}^{-1} \begin{pmatrix} l_{11} & l_{21} & l_{31} & l_{41} & l_{51} \\ 0 & l_{22} & l_{32} & l_{42} & l_{52} \\ 0 & 0 & l_{33} & l_{43} & l_{53} \\ 0 & 0 & 0 & l_{44} & l_{45} \\ 0 & 0 & 0 & 0 & l_{55} \end{pmatrix}^{-1} \begin{pmatrix} \sum_{k=1}^m (-u_0 + u_k) h_k \omega_k^2 \\ \sum_{k=1}^m (-u_0 + u_k) l_k \omega_k^2 \\ \sum_{k=1}^m (-u_0 + u_k) \frac{h_k^2}{2} \omega_k^2 \\ \sum_{k=1}^m (-u_0 + u_k) \frac{l_k^2}{2} \omega_k^2 \\ \sum_{k=1}^m (-u_0 + u_k) h_k l_k \omega_k^2 \end{pmatrix} \quad (141)$$

$$\begin{pmatrix} l_{11} & 0 & 0 & 0 & 0 \\ l_{21} & l_{22} & 0 & 0 & 0 \\ l_{31} & l_{32} & l_{33} & 0 & 0 \\ l_{41} & l_{42} & l_{43} & l_{44} & 0 \\ l_{51} & l_{52} & l_{53} & l_{54} & l_{55} \end{pmatrix}^{-1} \begin{pmatrix} l_{11} & l_{21} & l_{31} & l_{41} & l_{51} \\ 0 & l_{22} & l_{32} & l_{42} & l_{52} \\ 0 & 0 & l_{33} & l_{43} & l_{53} \\ 0 & 0 & 0 & l_{44} & l_{45} \\ 0 & 0 & 0 & 0 & l_{55} \end{pmatrix}^{-1} \triangleq \begin{pmatrix} c_{11} & c_{12} & c_{13} & c_{14} & c_{15} \\ c_{21} & c_{22} & c_{23} & c_{24} & c_{25} \\ c_{31} & c_{32} & c_{33} & c_{34} & c_{35} \\ c_{41} & c_{42} & c_{43} & c_{44} & c_{45} \\ c_{51} & c_{52} & c_{53} & c_{54} & c_{55} \end{pmatrix} \quad (142)$$

then

$$\begin{pmatrix} \frac{\partial u_0}{\partial x} \\ \frac{\partial u_0}{\partial y} \\ \frac{\partial^2 u_0}{\partial x^2} \\ \frac{\partial^2 u_0}{\partial y^2} \\ \frac{\partial^2 u_0}{\partial x \partial y} \end{pmatrix} = \begin{pmatrix} c_{11} & c_{12} & c_{13} & c_{14} & c_{15} \\ c_{21} & c_{22} & c_{23} & c_{24} & c_{25} \\ c_{31} & c_{32} & c_{33} & c_{34} & c_{35} \\ c_{41} & c_{42} & c_{43} & c_{44} & c_{45} \\ c_{51} & c_{52} & c_{53} & c_{54} & c_{55} \end{pmatrix} \begin{pmatrix} \sum_{k=1}^m (-u_0 + u_k) h_k \omega_k^2 \\ \sum_{k=1}^m (-u_0 + u_k) l_k \omega_k^2 \\ \sum_{k=1}^m (-u_0 + u_k) \frac{h_k^2}{2} \omega_k^2 \\ \sum_{k=1}^m (-u_0 + u_k) \frac{l_k^2}{2} \omega_k^2 \\ \sum_{k=1}^m (-u_0 + u_k) h_k l_k \omega_k^2 \end{pmatrix} \quad (143)$$

We consider $f_2(u) = \beta_1 \frac{\partial u}{\partial y}$ as a example, β_1 is a constant, and then

$$\begin{aligned} f_2(u) = & -u_0(\beta_1(\sum_{k=1}^m [c_{21} h_k \omega_k^2 + c_{22} l_k \omega_k^2 + c_{23} \frac{h_k^2}{2} \omega_k^2 + c_{24} \frac{l_k^2}{2} \omega_k^2 + c_{25} h_k l_k \omega_k^2])) \\ & + \sum_{k=1}^m [\beta_1(c_{21} h_k \omega_k^2 + c_{22} l_k \omega_k^2 + c_{23} \frac{h_k^2}{2} \omega_k^2 + c_{24} \frac{l_k^2}{2} \omega_k^2 + c_{25} h_k l_k \omega_k^2)] u_k. \end{aligned} \quad (144)$$

According to the explicit form of the generalized finite difference method(107), the coefficients m_0 and m_k are as follows,

$$m_0 = \beta_1(\sum_{k=1}^m [c_{21} h_k \omega_k^2 + c_{22} l_k \omega_k^2 + c_{23} \frac{h_k^2}{2} \omega_k^2 + c_{24} \frac{l_k^2}{2} \omega_k^2 + c_{25} h_k l_k \omega_k^2]), \quad (145)$$

$$m_k = \beta_1(c_{21} h_k \omega_k^2 + c_{22} l_k \omega_k^2 + c_{23} \frac{h_k^2}{2} \omega_k^2 + c_{24} \frac{l_k^2}{2} \omega_k^2 + c_{25} h_k l_k \omega_k^2), \quad (146)$$

that carries out condition $m_0 = \sum_{k=1}^m m_k$.

CRedit authorship contribution statement

Yanan Xing: Methodology, Writing the initial draft and the final draft. **Haibiao Zheng:** Methodology, Revising the paper.